

Managing public transit during a pandemic: the trade-off between safety and mobility

Qi Luo^{a,e}, Marissa Gee^b, Benedetto Piccoli^c, Daniel Work^d, Samitha Samaranyake^{a,b,*}

^a*School of Civil and Environmental Engineering, Cornell University, Ithaca, NY, USA*

^b*Center for Applied Mathematics, Cornell University, Ithaca, NY, USA*

^c*Department of Civil and Environmental Engineering, Vanderbilt University, Nashville, TN, USA*

^d*Department of Mathematical Sciences, Rutgers University, Camden, NJ, USA*

^e*Department of Industrial Engineering, Clemson University, Clemson, SC, USA*

Abstract

During a pandemic such as COVID-19, managing public transit effectively becomes a critical policy decision. On the one hand, efficient transportation plays a pivotal role in enabling the movement of essential workers and keeping the economy moving. On the other hand, public transit can be a vector for disease propagation due to travelers' proximity within shared and enclosed spaces. Without strategic preparedness, mass transit facilities are potential hotbeds for spreading infectious diseases. Thus, transportation agencies face a complex trade-off when developing context-specific operating strategies for public transit. This work provides a network-based analysis framework for understanding this trade-off, as well as tools for calculating targeted commute restrictions under different policy constraints, e.g., regarding public health considerations (limiting infection levels) and economic activity (limiting the reduction in travel). The resulting plans ensure that the traffic flow restrictions imposed on each route are adaptive to the time-varying epidemic dynamics. A case study based on the COVID-19 pandemic reveals that a well-planned subway system in New York City can sustain 88% of transit flow while reducing the risk of disease transmission by 50 % relative to fully-loaded public transit systems. Transport policy-makers can exploit this optimization-based framework to address health-and-economic trade-offs and make proactive transit management plans during an epidemic outbreak.

Keywords:

Public transit, Spatial compartmental model, Safety-and-mobility trade-off

1. Introduction

Operating public transit amid post-peak and post-epidemic periods is a double-edged sword: on the one hand, it provides basic and low-cost mobility services to those not owning cars or who place environmental concerns at the center of commuting decisions; on the other hand, human mobility, especially commuting by mass transit, contributes to the spatial propagation of infectious disease. Policy-makers face this *health-and-economic* trade-off when lifting the restrictions and restarting public transit systems during the unprecedented

*Corresponding author, samitha@cornell.edu

COVID-19 pandemic. There is evidence (van Dorn et al., 2020; Cohen and Kupferschmidt, 2020) that the epidemic outbreak had a disproportional impact on mass transit operators and passengers compared with other groups of the population. McLaren (2020) jointly analyzed census and mortality data and found that a significant portion of the racial disparity in COVID-19 deaths could be attributed to the use of public transit.

Due to safety concerns, many countries have implemented a temporary closure of transit systems (Lewnard and Lo, 2020); in some countries, ridership of public transit has dropped up to 90% (Amekudzi-Kennedy et al., 2020; DeWeese et al., 2020). While the potential risk of epidemic exposure inside subway carriages or buses has been well-recognized (Feng et al., 2020), there is a lack of scientific knowledge about the corresponding prevention strategies. This work aims to answer a critical question frequently raised by transportation agencies and researchers: How to control traffic flows in public transit networks to improve safety and preparedness during periods of spreading infection?

To answer this question, we first model the spread and mitigation of a particular epidemic disease through public transit networks using a metapopulation compartment model. The risk of disease transmission associated with public transit depends on the characteristics of the disease and the intervention policies implemented across the entire environment being modeled (Figure 1). In particular, we focus on movements between residences and work locations.¹ We propose a mathematical-programming based approach for designing targeted public transit policies, with the intent of minimizing the public health risk while maximizing mobility, in the context of dynamically evolving epidemics. We show that by applying targeted interventions on high-risk transit routes and regions, most inelastic travel demand can be satisfied while the spatial propagation of the infectious disease is restrained.

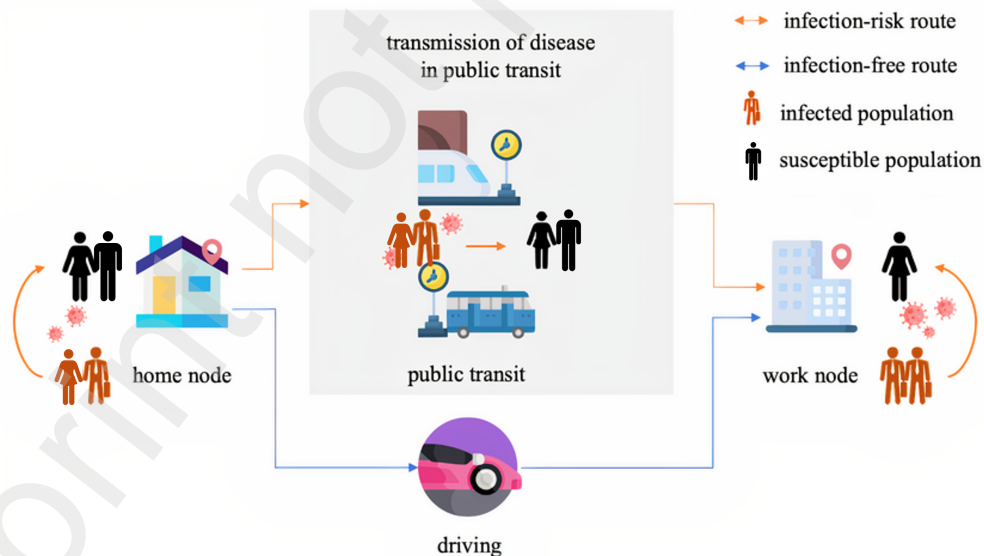


Figure 1: Illustration of transmission of infectious disease in public transit; Susceptible population is under the risk of infection in public-transit commuting trips and contacts in home and work regions.

¹We do so for simplicity of exposition and due to the detailed movement data available in this context. The model presented can be easily generalized to include other movements.

1.1. Objectives and main contributions

This work focuses on optimizing the commute networks' operations under disruptions caused by emerging infectious diseases. We are specifically interested in controlling the mobility patterns with dual objectives – providing reliable access to public transit services while slowing the communicable disease invasion.

The main contributions of this work are:

1. Developing an optimization-based analysis by integrating the spatial epidemic model and the commute network model.
2. Providing a forward-backward iterative method to solve the large-scale transit traffic control policies and obtain insight for effective interventions.
3. Investigating the optimal subway route operations plans in Manhattan, New York City (NYC) and evaluating the impact on COVID-19 pandemic transmission.

The method developed in this work can be applied to any infectious disease that can be potentially transmitted through public transit services, e.g., risk of aerosol and contact transmissions inside vehicles. The spatial epidemic model on the commute networks captures the influence of two most commonly implemented regulations: *quarantine* policies (population with severe symptoms is forced to stay at home) and *social-distancing* policies on public transit. Our work is one of the first attempts to investigate the transit traffic control policies with monitoring feedback considering the combined effects of repetitive commuting patterns and epidemic dynamics. The model developed in this work requires access to only publicly-available data and thus can be easily adopted by local transportation agencies to make data-driven responsiveness and preparedness plans.

1.2. Related work

There is a resurgence of interest in modeling the disease contagion processes associated with recurring commuting trips. The development of advanced metapopulation network models coincides with the pattern of increasingly frequent epidemics in recent years. Keeling et al. (2010) initiated the stream of network models for the spatial spreading of infectious disease in the commuter-to-work networks. They addressed that the infection dynamics in the recurrent commute networks were significantly different from their counterparts in the kernel and random mobility networks. Balcan and Vespignani (2011) drew a similar conclusion, whereas the diffusion rate and recurrent commuting rate jointly determine whether or not the global spreading of the infectious disease occurs. Bichara and Iggidr (2018) analyzed how the heterogeneous groups, patches, and mobility patterns affect the disease prevalence by a multi-group compartment model. Since the individual's commuting patterns are no longer random, Yashima and Sasaki (2016) found that the commute networks' topological characteristics such as the networks' degree distribution become relevant. When the degree of networks follows a heavy-tailed distribution, the disease invasion threshold decreases significantly. Hence, the epidemic is not preventable by merely random interventions such as quarantine and vaccination. Therefore, studying the relationship between commute networks and disease dynamics is of interest to epidemiology and transportation research.

A vast body of literature has extensively investigated transportation networks' operations after disruptions (e.g., natural disasters) and incidents such as strikes and epidemics as

in this work. As transportation systems are essential for the functioning of cities after disruptions, their resilience has become a key design principle (Zhou et al., 2019). This stream of work focuses on enhancing the networks' ability to maintain operations during the disruptive period or minimize the required resources for recovery. Note that the enhancement of transportation networks' resilience is only a derivative of measurements in prior work.

In an attempt to identify the risk of taking public transit during the outbreak of COVID-19, an infectious disease with millions of confirmed cases globally, Mo et al. (2020) proposed an individual encounter model that characterizes the transmission of the disease on public transportation facilities. As an agent-based model, the encounter model captures the probability of contact between individuals and thus evaluates the risk of transmitting disease from an infectious person to a susceptible one. They calibrated the model using the smart card data from Singapore. Using a similar approach, Qian et al. (2020) conducted a cross-city comparison of the contact networks using the smart card data from China. They constructed a universal generation model to explain the correlation between the metro contact network's properties and the risk level of transmissible diseases. Note these prior works all use the contact networks as the epidemic model to capture the social activity contacts; thus, rich trajectory data is required for model fitting. More importantly, these models only studied the spreading of the infectious disease in transit, ignoring the interactions between commuters and other residential population. Considering the short commuting period compared with other activities during the day, separating these two populations does not capture the long-tail implications of controlling traffic patterns. As a result, these models may underestimate the value of public transit intervention policies. Chang et al. (2020) combined the metapopulation model and commute networks to explain why the infection rates among disadvantaged groups were higher than the rest. Compared to agent-based models such as the individual encounter model, metapopulation models require access to demographic survey data that is normally publicly available.

Previous research typically only investigated the descriptive and predictive models, whereas this work aims to develop a prescriptive model for transit networks. The remaining paper is organized as follows. Section 2 blends the advances in the metapopulation epidemic models with the network fortification models. The resulting optimization lays the foundation for making transportation policy that balances the need to return to normal activities and prevent public health hazards. Section 3 derives general rules for managing public transit under public health measures. Section 4 implements this model in a case study of New York City's subway systems and tests the public transit control policy's impact on spreading the contagious disease. Section 5 draws the final conclusion.

2. Methodology

2.1. Metapopulation model for commute networks

This work focuses on the recurring commuting trips, which account for 79% of all transit trips in the United States (including work and school trips) (Lee and Hickman, 2014). Commuting remains the primary demand for traveling during the epidemic period and revives rapidly in reopening the economy (Wang et al., 2020; Hu et al., 2020).

The commute mobility patterns are mainly modeled by the following three approaches. First, we may model the movement in urban commute networks on the individual level.

Reconstructing the contact networks requires access to massive human motion trajectory data notwithstanding (Mo et al., 2020). Tracking passengers’ use of public transit and alternative modes is costly. Thus, any control policies derived from the contact networks are slow to implement, occasionally impossible due to privacy concerns, and biased due to the limited electronic device users.

The second approach for modeling traveling patterns is random mobility models. These models assume that passengers follow certain movement distributions such as random walk over the network. Nevertheless, prior work has revealed that recurring commute trips (i.e., individuals take the fixed routes back and forth) significantly impact the disease dynamics and the derived control policies (Keeling et al., 2010). Therefore, random mobility models are not suitable for public transit applications and developing safe and effective transit control policies based on movement data.

A third option that is promising is the use of metapopulation models. First, conventional transportation planning has been using basic geography units such as traffic analysis zones (TAZ) or census tracts, so considerable resources and datasets are already in local transportation agencies’ hands. A vast stream of literature has developed fundamental methods for generating and analyzing these grid-based models. Second, leveraging the richness of urban planning and transportation models associated with these basic geography units, researchers can explore the connections to commuters’ demographic features to develop context-specific plans in preventing epidemics. For example, how to connect the use of public transport to the racial disparities (McLaren, 2020). Finally, epidemic response policies and guidance are often made on a macroscopic network level. In what follows, we introduce how to construct such a metapopulation model for a public transit system (called “commute network” throughout this paper). All the notation used in the paper is summarized in Table A.2 in Appendix A.

During the day, each resident is in one of three statuses: at home (“ H ”), at work (“ W ”), or commuting (“ C ”). A commute network integrates two separate systems: a home-and-work network $\mathcal{G}_{HW} = (\mathcal{V}_{HW}, \mathcal{E}_{HW})$ consisting of basic geography units such as census tracts or TAZs, and public transit networks $\mathcal{G}_C = (\mathcal{V}_C, \mathcal{E}_C)$ serving daily commute between these home-and-work regions (Figure 2).

1. Home-and-work network \mathcal{G}_{HW} :

- (a) Residents live in a closed complete network with a fixed population $N_v \in \mathbb{Z}^+$ for each $v \in \mathcal{V}_{HW}$. We denote $\mathbf{N} = [N_v]_{v \in \mathcal{V}_{HW}}$ whenever there is no possibility of confusion.
- (b) Each region $v \in \mathcal{V}_{HW}$ has a set of neighboring outflow regions $\mathcal{N}^+(v) := \{u \in \mathcal{V}_{HW} : (v, u) \in \mathcal{E}_{HW}\}$ and a set of inflow regions $\mathcal{N}^-(v) := \{u \in \mathcal{V}_{HW} : (u, v) \in \mathcal{E}_{HW}\}$. The fraction of residents at v travels to $u \in \mathcal{N}^+(v)$ is $r_{vu} \in [0, 1]$. Flow conservation ensures that the fractions satisfy $\sum_{u \in \mathcal{N}^+(v)} r_{vu} = 1$ for all $v \in \mathcal{V}_{HW}$.

2. Public transit network \mathcal{G}_C :

- (a) \mathcal{V}_C represents a set of public transit routes available to commuters. Each *route* may contain a single public transit line or transfers between multiple modes or lines.
- (b) Expanding $\mathcal{V} = \mathcal{V}_{HW} \cup \mathcal{V}_C$ such that edges \mathcal{E}_C connect each region $v \in \mathcal{V}_{HW}$ to accessible routes $w \in \mathcal{V}_C$.

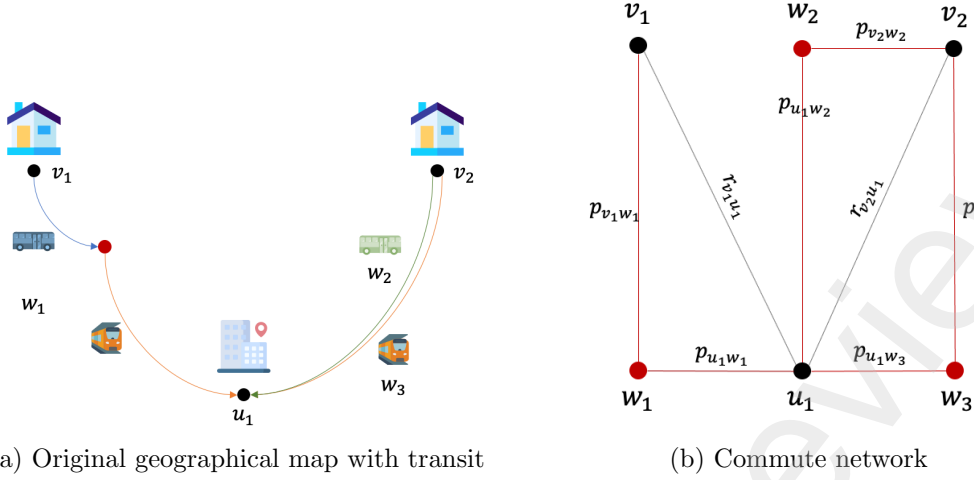


Figure 2: Construct commute network by integrating home-and-work network and public transit network

(c) We define the outflow and inflow to public transit as $\mathcal{C}^+(v)$ and $\mathcal{C}^-(v)$, respectively, upon edges \mathcal{E}_C . The fraction of population living in $v \in \mathcal{V}_{HW}$ takes the route $w \in \mathcal{V}_C$ is $p_{vw} \in [0, 1]$. The summation of fractions $\sum_{u \in \mathcal{C}^+(v)} p_{vu} \leq 1$ holds for all $v \in \mathcal{V}$ if $\mathcal{C}^+(v) \neq \emptyset$ because residents can choose other modes of transport such as walking or driving.

3. Effective population:

- (a) We define the effective work-time population as $N_v^e(t) := \sum_{u \in \mathcal{N}^-(v)} r_{uv} N_u$.
- (b) The effective commuting population as $C_v^e(t) := \sum_{w \in \mathcal{C}^-(v)} p_{vw} N_v(t)$ by assuming that commuters take the same route back and forth so that $p_{vw} = p_{vw}$ for any $w \in \mathcal{C}^-(v)$.
- (c) Let ρ_N and ρ_C be the traffic flow fraction matrix r_{uv} for the home-and-work and p_{vu} for the the public transit network, respectively. We can rewrite the effective population as $N^e(t) = \rho_N^T N(t)$ and $C^e(t) = \rho_C^T N(t)$.

We call the integration of the two networks a *commute network* $\mathcal{G} = (\mathcal{V}, \mathcal{E})$. The *route* is represented as a vertex in commute networks because contagious diseases such as COVID-19 can spread via respiratory, aerosol, or contact transmission in vehicles. Experiments have shown that the infectious virus particles can be detected from surfaces for up to 24 hours or even three days (Van Doremalen et al., 2020; Chin et al., 2020). These results imply that travelers may be exposed to the disease in a carriage carrying infectious passengers at different times. Since the risk of being exposed is possibly exceeding direct personal contact, the metapopulation model has captured the average effect of the infection in the daily use of transit service.

A common concern is that the traveling behavior may shift away from public transit systems because of the epidemic outbreak (Wang et al., 2020), and the government's disease control plans, such as reducing the public transit service time or alternative seating, exacerbate this trend. In addition, travelers may switch to a different mode, take a different route, or follow different schedules to avoid contacting potentially infectious population. The travel rate p_{vu} for each $v \in \mathcal{V}_{HW}$ and $u \in \mathcal{C}^+$ implicitly incorporates a mix of route and mode

choices. Since factors such as traveling time and trip purpose still play a central role in these distributions during an epidemic, this work uses fixed fractions p_{vu} throughout the analysis. Estimating travel behavior changes requires new empirical research using post-epidemic data and is beyond the scope of this work.

2.2. Spatial epidemic model

Spatial epidemic models are widely used to model the spread of infectious disease and quantify workable disease control strategies. Many infectious diseases have an extended period from infection to onset of symptoms, which causes a significant challenge in addressing control strategies. For example, the respiratory symptoms of COVID-19 appear in as few as two days or as long as 14 days after exposure (Chin et al., 2020). To capture this feature, we use a standard metapopulation SEIR epidemic model that divide the population at time $t \in \mathbb{R}_+$ at each vertex, $N_v(t)$, into four groups, susceptible, exposed, infectious, and recovered as $S_v(t), E_v(t), I_v(t)$, and $R_v(t)$, respectively; i.e., $N_v(t) = S_v(t) + E_v(t) + I_v(t) + R_v(t)$ for all $v \in \mathcal{V}_{HW}$. In addition to these compartments, we track the proportion of cases that are symptomatic, which we denote as $\alpha(t)$. In each period, the symptomatic infectious population $Q_v(t) = \alpha(t)I_v(t)$ is assumed to be quarantined in the home region v . The quarantined population is isolated from the rest while the non-symptomatic individuals, $(1 - \alpha(t))I_v(t)$, continue to move in commute networks. The standard SEIR model is presented in Figure 3.

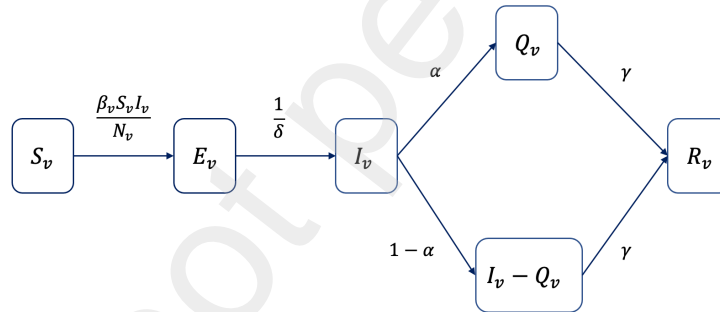


Figure 3: SEIR model on commute networks under quarantine policies.

The transmission of the disease is captured by three parameters in the SEIR model: the contact rate β_v (the average number of contacts per person per time), the mean latent period $1/\delta$, and the recovering rate γ . The contact rate β_v is vertex-dependent because different regions $v \in \mathcal{V}_{HW}$ and public transit lines $v \in \mathcal{V}_C$ may employ different risk mitigation measures.

The Spatial SEIR model expands the aggregate SEIR model to commute networks using a graph-representation in Mori et al. (2020). The dynamics of the susceptible population, i.e., the rate of becoming exposed once having infectious contact with the infected population,

is described as follows:

$$\begin{aligned} \frac{dS_v(t)}{dt} = & -p_H S_v(t) \left(\frac{(1-\alpha(t))\beta_v I_v(t)}{N_v} \right) - p_W S_v(t) \left(\sum_{u \in \mathcal{N}^+(v)} \frac{(1-\alpha(t))r_{vu}\beta_u [\rho_N I(t)]_u}{[\rho_N N]_u} \right) \\ & - p_C S_v(t) \left(\sum_{w \in \mathcal{C}^+(v)} \frac{(1-\alpha(t))p_{vw}\beta_w [\rho_C I(t)]_w}{[\rho_C N]_w} \right), \end{aligned} \quad (1)$$

where p_H, p_C and p_W represent the fraction of time during the day involving staying in the home region, commuting, and in the workplace, respectively. These three terms calculate the probability of being exposed in the home region, work region, and while taking public transit, respectively. As in the standard SEIR model, $(1-\alpha(t))$ percentage of the infected population is isolated at their home region. Note that $\sum_{v \in \mathcal{V}_{HW}} [\rho_C^\top N]_v \leq \sum_{v \in \mathcal{V}_{HW}} N_v$ as we do not assume that every trip (u, v) is carried by public transit, and choosing other modes such as driving bear no risk of contagion in commuting.

The Spatial SEIR model on commute networks can be written in a compact matrix form:

$$\begin{aligned} \frac{\partial \mathbf{S}_t}{\partial t} &= -p_H \mathbf{S}_t^\top \mathbf{I}_t^H - p_W \mathbf{S}_t^\top \mathbf{I}_t^W - p_C \mathbf{S}_t^\top \mathbf{I}_t^C, \\ \frac{\partial \mathbf{E}_t}{\partial t} &= -\frac{\partial \mathbf{S}_t}{\partial t} - \frac{1}{\delta} \mathbf{E}_t, \\ \frac{\partial \mathbf{I}_t}{\partial t} &= \frac{1}{\delta} \mathbf{E}_t - \gamma \mathbf{I}_t \\ \frac{\partial \mathbf{R}_t}{\partial t} &= \gamma \mathbf{I}_t, \end{aligned} \quad (2)$$

The Spatial SEIR model guarantees that $dN_v/dt = 0$ for each $v \in \mathcal{V}_{HW}$ and $t \in \mathbb{R}^+$. These population vectors are given by:

$$\begin{aligned} \mathbf{S}_t &= [S_v(t)]_{v \in \mathcal{V}}^\top, & \mathbf{E}_t &= [E_v(t)]_{v \in \mathcal{V}}^\top, \\ \mathbf{I}_t &= [I_v(t)]_{v \in \mathcal{V}}^\top, & \mathbf{R}_t &= [R_v(t)]_{v \in \mathcal{V}}^\top, \\ \begin{cases} \mathbf{I}_t^H &= [\beta_v \frac{I_v(t)}{N_v}]_{v \in \mathcal{V}}^\top \\ \mathbf{I}_t^W &= [\sum_{u \in \mathcal{N}^+(v)} r_{vu}\beta_u \frac{(1-\alpha(t))[\rho_N I(t)]_u}{[\rho_N N]_u}]_{v \in \mathcal{V}}^\top \\ \mathbf{I}_t^C &= [\sum_{w \in \mathcal{C}^+(v)} p_{vw}\beta_w \frac{(1-\alpha(t))[\rho_C I(t)]_w}{[\rho_C N]_w}]_{v \in \mathcal{V}}^\top \end{cases} \end{aligned}$$

We can obtain the *basic reproduction number* R_0 from the epidemic dynamics, which is a critical measurement to guide disease control. R_0 is the average number of secondary cases produced by one infected individual introduced into a completely susceptible population (Yashima and Sasaki, 2016). Emerging infectious diseases such as COVID-19 spread more rapidly in a region if R_0 is large. In addition, R_0 also determines what proportion of the population should be immunized or vaccinated to eradicate the infectious disease.

The basic reproduction number R_0 is calculated by the dominant eigenvalue of the *next generation matrix* (NGM) $G_0 \in \mathbb{R}^{|\mathcal{V}_{HW}| \times |\mathcal{V}_{HW}|}$. The epidemic dynamics described by eq.(2) can be split into two parts (a) the rate of appearance of new infections in compartments

denoted as a matrix F , and (b) the rate of transfer into compartments denoted as a matrix V . NGM is defined by $G_0 = FV^{-1}$. The derivation of NGM for the Spatial SEIR model is a tedious but crucial task for the remainder of this paper. We describe how to compute the Jacobian matrix of the equation system eq.(2) and the explicit expression of NGM in Appendix B.

The time-varying measures of the disease reproduction rate in a partially susceptible population is measured by the *effective reproduction number* R_t , which is the dominant eigenvalue of effective NGM G_t at time $t \in \mathbb{R}_+$. We can take a shortcut by obtaining the expression for changes in R_t as a result of parameter changes in the epidemic model. For a fixed time t , let ζ and η be the eigenvectors associated with R_t in the eigenvector decomposition of G_t , i.e., $\zeta^\top G_t = R_t \zeta^\top$, $G_t \eta = R_t \eta$, and normalized such that $\zeta^\top \eta = 1$. If we vary the Spatial SEIR model parameters by controlling the transit ridership through the planning horizon, we can evaluate the change of the reproduction number as:

$$\Delta R_t = \frac{\zeta^\top \Delta G_t \eta}{\zeta^\top \eta}. \quad (3)$$

2.3. Optimizing transit flows with disease reproduction constraints

The control for this public transit system is how to curb traffic flows on particular routes to balance the increasing commuting demand and the hastening spreading of infectious disease. For each $u \in \mathcal{V}_{HW}$, $w \in \mathcal{V}_C$, we let $x_{uw} \in [0, 1]$ denote the proportion of subpopulation allowed to use this public transit route. Such a control can be realized by reducing service frequency on a particular route, imposing capacity regulations inside public transit vehicles, or limiting capacity at these transit stops. In the fixed flow control case, \mathbf{x} is fixed at time $t = 0$; in the extended version, the policy-maker adaptively changes the guidance for using public transit $\mathbf{x}(t)$ after observing that R_0 hits certain thresholds over the planning horizon $t \in [0, T]$.

2.3.1. Fixed flow control policy

Our decision $\mathbf{x} \in \mathbb{R}^{|\mathcal{V}_{HW}| \times |\mathcal{V}_C|}$ is the proportion of flows allowed to use public transit on each route (v, w) , $v \in \mathcal{V}_{HW}$, $w \in \mathcal{V}_C$. Our primary goal is to set an initial control plan throughout $[0, T]$ to maximize the transit network's throughput while protecting the public from the risk of exposure to infectious diseases. We can formulate the problem as follows:

$$\begin{aligned} & \text{maximize}_{\mathbf{x}} && \sum_{(v,w):v \in \mathcal{V}_{HW}, w \in \mathcal{V}_C} x_{vw} p_{vw} N_v && (4) \\ \text{s.t.} & && \Delta R_0(\mathbf{x}) \leq \kappa(R_0(1) - R_0(0)) \\ & && 0 \leq x_{vw} \leq 1, && \forall v \in \mathcal{V}_{HW}, \forall w \in \mathcal{V}_C. \end{aligned}$$

The right-hand side of the disease reproduction constraint in eq.(4) means that the change of basic reproduction number due to opening public transit is within a tolerance $\kappa \in [0, 1]$ from the worst case. The worst case is measured by R_0 with the full reopening of transit ($\mathbf{x} = 1$ called the ‘‘control-free’’ case) and the best case is with no opening of transit at all ($\mathbf{x} = 0$ called the ‘‘shutdown’’ case). Lemma 2 gives a more rigorous proof. Despite the fact that this constraint can be explicitly calculated by eq.(3), we use this relative measure of

the disease spreading because of the instability of input data. The exact values of NGM are sensitive to input data, such as the epidemic model's parameters and route choice estimation in the metapopulation model. In contrast, the relative value of $R_0(1) - R_0(0)$ is a stable measure, and the derived control policy is more robust to the modeling errors.

The explicit expressions of constraints are derived from the NGM in Appendix B. Assuming a constant quarantine ratio of α , the NGM under control policy \mathbf{x} at time t , $G_t(\mathbf{x})$, can be computed from the production of *transmission* and *transition* matrices. For each tuple of $u, v \in \mathcal{V}_{HW}$, we have:

$$\begin{aligned} [G_t(\mathbf{x})]_{vv} &= \frac{1}{\gamma} \left[p_H \beta_v (1 - \alpha) \frac{S_v(t)}{N_v} + p_W \sum_{u \in \mathcal{N}^+(v)} r_{vu}^2 \beta_u \frac{(1 - \alpha) S_v(t) [\rho_N^\top N]_u}{([\rho_N^\top N]_u)^2} + \right. \\ &\quad \left. p_C \sum_{w \in \mathcal{C}^+(v)} x_{vw}^2 p_{vw}^2 \beta_w \frac{(1 - \alpha) S_v(t) [\rho_C(\mathbf{x})^\top N]_w}{([\rho_C(\mathbf{x})^\top N]_w)^2} \right], \\ [G_t(\mathbf{x})]_{vu} &= \frac{1}{\gamma} \left[p_W \sum_{w \in \mathcal{N}^+(u) \cap \mathcal{N}^+(v)} r_{uw} r_{vw} \beta_w \frac{(1 - \alpha) S_v(t) [\rho_N^\top N]_w}{([\rho_N^\top N]_w)^2} + \right. \\ &\quad \left. p_C \sum_{w \in \mathcal{C}^+(u) \cap \mathcal{C}^+(v)} x_{uw} p_{uw} x_{vw} p_{vw} \beta_w \frac{(1 - \alpha) S_v(t) [\rho_C(\mathbf{x})^\top N]_w}{([\rho_C(\mathbf{x})^\top N]_w)^2} \right]. \end{aligned}$$

With fixed \mathbf{x} over the planning horizon $t \in [0, T]$, the disease reproduction constraint in eq.(4) is given by:

$$\zeta^\top (G_0(\mathbf{x}) - G_0(0)) \eta \leq (R_0(1) - R_0(0)) \zeta^\top \eta, \quad (5)$$

where $[G_0(\mathbf{x}) - G_0(0)]_{vu} =$

$$\begin{cases} p_C \sum_{w \in \mathcal{C}^+(v)} x_{vw}^2 p_{vw}^2 \beta_w (1 - \alpha) \frac{S_v}{[\rho_C(\mathbf{x})^\top N]_w} & , v = u \\ p_C \sum_{w \in \mathcal{C}^+(u) \cap \mathcal{C}^+(v)} x_{uw} p_{uw} x_{vw} p_{vw} \beta_w (1 - \alpha) \frac{S_v}{[\rho_C(\mathbf{x})^\top N]_w} & , v \neq u. \end{cases}$$

Given controls \mathbf{x} , there exists an obvious disease-free equilibrium $S_v(0) = N_v$ and $I_v(0) = 0$ for all $v \in \mathcal{V}$ at $t = 0$. We can further simplify eq.(5) as:

$$[G(\mathbf{x}) - G(0)]_{vu} = \begin{cases} p_C (1 - \alpha) N_v \sum_{w \in \mathcal{C}^+(v)} \frac{x_{vw}^2 p_{vw}^2 \beta_w}{[\rho_C(\mathbf{x})^\top N]_w} & , v = u \\ p_C (1 - \alpha) N_v \sum_{w \in \mathcal{C}^+(u) \cap \mathcal{C}^+(v)} \frac{x_{uw} p_{uw} x_{vw} p_{vw} \beta_w}{[\rho_C(\mathbf{x})^\top N]_w} & , v \neq u. \end{cases} \quad (6)$$

It is important to address that the optimal transit control policy computed above has limitations for the following reasons. First, we assume that commuters' choice of alternative modes of transport (e.g., driving, walking, ride-hailing) is risk-free from contagious disease throughout the analysis. Potential commuters disregard the travel plans if no option is available. Second, the control plan \mathbf{x} is implemented at $t = 0$ and remains the same throughout the planning horizon. This static policy is suboptimal in the face of infectious disease's evolving conditions. We propose a more general control policy in the next section.

2.3.2. Flow control with monitoring feedback

In the course of disease preparedness plans, transportation planning authorities need to make sequential decisions during $[0, T]$ when there is an evolving situation with regards to an infectious disease. Since the basic reproduction number $R_t(x(t))$ represents the expected future infections after adopting the public transit control $x(t)$, we intend to design a control policy adaptive to the progress of the infectious disease. The optimal control policy is derived by solving the following extension of eq.(4):

$$\begin{aligned} & \text{maximize } \sum_{\tau \in \mathbf{T}} \sum_{(v,w): v \in \mathcal{V}_{HW}, w \in \mathcal{V}_C} x_{vw}(\tau) p_{vw} N_v \cdot \Delta\tau & (7) \\ \text{s.t. } & \Delta R_\tau(\mathbf{x}(\tau)) \leq \kappa_{R_\tau(0), R_\tau(1)}(\tau) [R_\tau(1) - R_\tau(0)], & \forall \tau \in \mathbf{T}, \\ & 0 \leq x_{vw} \leq 1, & \forall v \in \mathcal{V}_{HW}, \forall w \in \mathcal{V}_C. \end{aligned}$$

The objective function is the cumulative network throughput over $t \in [0, T]$. In the transition from the widespreading of the infectious disease to reopening of economy, the policy-maker prefers to set a series of thresholds of κ with regard to R_t and wants to determine corresponding transit control policies at periods $\mathbf{T} = \{0, \tau_1, \dots, T\}$. This corresponds to the public transit operator's intention to lift the safety measures after the spreading of the disease has slowed down. The disease reproduction constraint guarantees that this sequence of health measures regarding R_τ is preserved at time $\tau \in \mathbf{T}$, and each control $\mathbf{x}(\tau)$ persists for $\Delta\tau$ periods. As a result, this constraint is adaptive to the impact of transit control policy up to time τ . Note that $\kappa_{R_t(0), R_t(1)}(t)$ is dependent on the values realized at period t . Since the fixed flow control policy is a special case of the multi-stage policy with monitoring feedback by setting $\mathbf{T} = \{0, T\}$ and $\mathbf{x}(\tau) = \mathbf{x}$, this derived policy is more effective than the policies in eq.(4). On the contrary, the fixed policy is simpler to calculate and implement. Hence, we use the fixed control policy as a starting point for the multistage control with monitoring feedback in Algorithm 1.

Algorithm 1 Public transit flow control with monitoring feedback

Initial SEIR model $\mathbf{S}_0, \mathbf{E}_0, \mathbf{I}_0, \mathbf{R}_0$, population N , and network flow r over the commute network.

Solve fixed control problem $\hat{\mathbf{x}}$ and set the optimal control $\mathbf{x}(\tau) \leftarrow \hat{\mathbf{x}}$ for all $\tau \in \mathbf{T}$.

while $t \leq T$ **do**

$\mathbf{x}(\tau) = \hat{\mathbf{x}}$ for $\tau < t$

 Let $t \leftarrow t + \Delta t$:

 · Forward step: Simulate spatial SEIR model and obtain \mathbf{S}_t and \mathbf{I}_t .

 · Backward step: Solve the subproblems of optimization in eq.(7) with $\mathbf{T} = [t, T]$ to obtain the optimal control $\mathbf{x}^*(\tau), \tau \geq t$ and optimal value $OPT(t)$.

Ensure: $\Delta R_\tau(\mathbf{x}) \leq \kappa(\tau)(R_\tau(1) - R_\tau(0))$ for all $\tau \geq t$

 Update control by $\mathbf{x}(t) \leftarrow \mathbf{x}^*(t)$

 Update the objective value $OPT \leftarrow OPT(t)$

end while

return $\mathbf{x}(t)$ for $t \in \mathbf{T}$ and the corresponding optimal value OPT .

Solving control at $t = [0, T]$ is more challenging due to the confounding simulation-and-optimization issue. Given policy $\mathbf{x}(\tau)$, simulating the spatial SEIR model and compute the trajectory of disease outbreak following this policy is time-consuming and control-dependent. The workload grows exponentially when the length of R_t threshold list increase. This imposes a need to reduce the enumeration of controls by separating the simulation and optimization compounds using the following procedure in Algorithm 1.

We initialize the algorithm with the optimal fixed control policy. Then, in each backward step, we update the control policy after the current period and simulate the epidemic dynamics up to the current period. This procedure is valid because R_t is a long-term measure for the outbreak of contagious disease under prior controls. Given a sequence of controls along \mathbf{T} , the disease reproduction constraints have a knapsack structure, and the objective function is a linear combination of realized network throughput. Nevertheless, the procedure is suboptimal because we do not enumerate all possible states of \mathbf{S}_t and \mathbf{I}_t as evaluating each policy is costly. It is worth noticing that the disease reproduction constraints in optimization eq.(4) and eq.(7) are non-convex and the dimension of $\mathbf{x} \in \mathbb{R}^{|\mathcal{V}_{HW}| \times |\mathcal{V}_C|}$ is large.

In practice, we can integrate the sequential data collection into the aforementioned analysis as follows:

1. At each period $\tau \in \mathbf{T}$, the observed infectious statistics is used to calibrated the epidemic model $(\mathbf{S}_t, \mathbf{E}_t, \mathbf{I}_t, \mathbf{R}_t)$.
2. If interventions starts in the middle of disease outbreak at period \tilde{t} and controls were not available in the early stage, we set $\mathbf{x} = 1$ for periods $[0, \tilde{t}]$ and resolve the control problem with monitoring feedback for periods $[\tilde{t}, T]$.

3. General rules for public transit control policy

This section specifies the existence conditions for optimal control and highlights the special structure and general rules for the optimal transit flow control policies. For ease of analysis, we study the fully connected commute networks where each home region is reachable from other work regions, and each commute region in \mathcal{V}_C connects to all regions in \mathcal{V}_{HW} . This connectivity assumption does not lose generality because we can model inaccessible routes by enforcing zero flow. The expanded network $(\mathcal{V}, \mathcal{E})$ based on transit route is not fully connected as not each pair routes are connected. The following lemma provides the existence conditions for optimal fixed control policy.

Lemma 1. *If the operator uses a global proportional control on public transit flow, i.e., x_{vw} is a constant for all $v \in \mathcal{V}_{HW}$ and $w \in \mathcal{V}_C$, the change of basic reproduction number is proportional to the control-free case with the same constant.*

Proof. Let set $x_{vw} = \sigma$ for all $v \in \mathcal{V}_{HW}$ and $w \in \mathcal{V}_C$, which means that we allow a constant ratio of residents to use public transit on each route. We have $\rho_C(\mathbf{x}) = \sigma \rho_C(1)$, and hence $\rho_C(\mathbf{x})^\top N = \sigma \rho_C(1)^\top N$ and $\frac{x_{vw}}{[\rho_C(\mathbf{x})^\top N]_w} = \frac{1}{[\rho_C(1)^\top N]_w}$. Since $\frac{x_{vw}}{[\rho_C(\mathbf{x})^\top N]_w}$ appear in each entry of eq.(6), we have $\sigma[G(1) - G(0)] = G(\mathbf{x}) - G(0)$ and $\sigma[R_0(1) - R_0(0)] = R_0(\mathbf{x}) - R_0(0)$. \square

It is worth noting that this lemma is true because we assume that people have access to alternative modes for commuting. Lemma 1 is an important building block for solving

optimization in eq.(4) and eq.(7) because it means that, for any exogenous κ , we can set $\mathbf{x} = \kappa$ to satisfy the constraints. In other words, the feasible set of the optimization problem is nonempty.

Definition 1. A control policy \mathbf{x} is more restrained than \mathbf{x}' if:

1. $x_{vw} \leq x'_{vw}$ for all $v \in \mathcal{V}_{HW}$ and $w \in \mathcal{V}_C$ and there exists edges such that $x_{vw} < x'_{vw}$.
2. Each pair of $x_{vw} > 0, x_{uw} > 0$ has dominating marginal effect on the controlled routes (v, w) and (u, w) with regard to the effective population, i.e., $\frac{x'_{vw}x'_{uw}}{x_{vw}x_{uw}} \geq \frac{[\rho_C(\mathbf{x}')^\top N]_w}{[\rho_C(\mathbf{x})^\top N]_w}$.

We then have the following lemma:

Lemma 2 (Monotonicity). *If a public transit control policy \mathbf{x} is more restrained than \mathbf{x}' , then $R_0(\mathbf{x}) < R_0(\mathbf{x}')$.*

Proof. Without loss of generality, we assume the NGM associated with \mathbf{x} and \mathbf{x}' both have linearly independent eigenvectors. NGM is nonnegative real-valued. We let the two NGM be $G := G_t(\mathbf{x})$ and $G' := G_t(\mathbf{x}')$. The difference $G' - G$ in each entry is:

$$\begin{cases} (1 - \alpha)N_v p_C \sum_{w \in \mathcal{C}^+} \beta_w p_{vw}^2 \left[\frac{x'_{vw}}{[\rho_C(\mathbf{x}')^\top N]_w} - \frac{x_{vw}}{[\rho_C(\mathbf{x})^\top N]_w} \right], & u = v \\ (1 - \alpha)N_v p_C \sum_{w \in \mathcal{C}^+} \beta_w p_{vw} p_{uw} \left[\frac{x'_{vw}x'_{uw}}{[\rho_C(\mathbf{x}')^\top N]_w} - \frac{x_{vw}x_{uw}}{[\rho_C(\mathbf{x})^\top N]_w} \right], & u \neq v. \end{cases}$$

Let $\mathbf{x}' = \mathbf{x} + \boldsymbol{\sigma}$. For an arbitrary $w \in \mathcal{V}_C$, we can plug \mathbf{x}' into $G' - G$ so we can represent the NGMs as $G' = G + \boldsymbol{\sigma}'G$ with a relatively small perturbation $\boldsymbol{\sigma}'G$. We can observe that, if the conditions of restrained controls are satisfied, then each term above is nonnegative. Note that $\boldsymbol{\sigma}'G \geq 0$ is a function of $\boldsymbol{\sigma}$ and x . According to the matrix perturbation theory (Bhatia, 2007), we have $\lambda'_i = \lambda_i + \eta_i^\top \boldsymbol{\sigma}'G \eta$ for each eigenvalue λ_i . By definition, R_0 is the largest eigenvalue of NGM and we conclude that $R_0(\mathbf{x}') > R_0(\mathbf{x})$. \square

Remark 1. *Lemma 2 indicates that reducing the traffic flow on a particular public transit route does not necessarily reduce $R_0(\mathbf{x})$.*

This remark emphasizes the importance of solving a global optimization for transit flow control to slow down the spreading of the infectious disease. Lemma 2 is not true if only condition 1 of restrained control holds. A counterexample is as follows. Instead of computing $\boldsymbol{\sigma}'G$, we only need to show that, for any given \mathbf{x} and arbitrary $u \in \mathcal{V}_{HW}, v \in \mathcal{V}_{HW}$, we have

$$[\boldsymbol{\sigma}'G]_{vu} = \frac{(x_{vw} + \sigma_{vw})(x_{uw} + \sigma_{uw})}{[\rho_C(\mathbf{x})^\top N + \rho_C(\boldsymbol{\sigma})^\top N]_w} - \frac{x_{vw}x_{uw}}{[\rho_C(\mathbf{x})^\top N]_w}.$$

We can easily find $\sigma_{vw} > 0, \sigma_{uw} > 0$ such that $[\boldsymbol{\sigma}'G]_{vu} < 0$ by having a third vertex v' with $N_{v'}\sigma_{v'w} \gg \sigma_{vw} + \sigma_{uw}$. Hence $R_0(\mathbf{x})$ increases with \mathbf{x} . The optimization problem eq.(4) is thus non-trivial because we cannot use gradient-based search method or split the problem by column decomposition.

A disease-free equilibrium of the Spatial SEIR model is obtained by setting $\mathbf{I}_t = 0$ and $\mathbf{S}_t = \mathbf{N}$. At this equilibrium, the expressions for G and $R_0(\mathbf{x})$ simplify dramatically, and can be used to obtain interpretable bounds on $R_0(\mathbf{x})$ and $\Delta R_0(\mathbf{x})$. The asymmetry between

the home-and-work network and commute network motivates the derivation of the following general rules for obtaining upper-bounds on the public transit operations. First, we examine the behavior of $R_0(\mathbf{x})$.

Theorem 1. *At the disease free equilibrium, with intervention \mathbf{x} , we have*

$$R_0(\mathbf{x}) \leq \frac{1-\alpha}{\gamma} \max_{v \in \mathcal{V}_{HW}} \left[p_H \beta_v + p_W \sum_{w \in N^+(v)} r_{vw} \beta_w + p_C \sum_{w \in C^+(v)} x_{vw} p_{vw} \beta_w \right]. \quad (8)$$

Proof. Since $R_0(\mathbf{x})$ is the spectral radius of $G(\mathbf{x})$, we have $R_0(\mathbf{x}) \leq \|G(\mathbf{x})\|$ for any induced matrix norm. Choosing the ℓ^1 norm, we have

$$R_0(\mathbf{x}) \leq \|G_0\|_{\ell^1} = \max_{v \in \mathcal{V}_{HW} \cup \mathcal{V}_C} \sum_{u=1}^n [G_0(\mathbf{x})]_{uv}.$$

Computing the sum of the entries for each column v of $G_0(\mathbf{x})$, we obtain

$$\begin{aligned} \sum_{u=1}^n [G_0(\mathbf{x})]_{uv} &= \frac{p_H(1-\alpha)}{\gamma} \beta_v + \frac{p_W(1-\alpha)}{\gamma} \sum_{u=1}^n \sum_{w=1}^n r_{uw} r_{vw} \beta_w \frac{N_u}{[\rho_N^\top N]_w} \\ &\quad + \frac{p_C(1-\alpha)}{\gamma} \sum_{u=1}^n \sum_{w=1}^m x_{uw} p_{uw} x_{vw} p_{vw} \beta_w \frac{N_u}{[\rho_C(\mathbf{x})^\top N]_w} \\ &= \frac{p_H(1-\alpha)}{\gamma} \beta_v + \frac{p_W(1-\alpha)}{\gamma} \sum_{w=1}^n r_{vw} \beta_w + \frac{p_C(1-\alpha)}{\gamma} \sum_{w=1}^m x_{vw} p_{vw} \beta_w. \end{aligned}$$

Taking the maximum over v gives the desired expression. □

Remark 2. *This bound in eq.(8) can be further simplified to*

$$R_0(\mathbf{x}) \leq \frac{(1-\alpha) \max_{v \in \mathcal{V}_{HW} \cup \mathcal{V}_C} \beta_v}{\gamma} \left(p_H + p_W + p_C \max_{v,w} x_{vw} \right),$$

which makes clear the relationship to R_0 in the single population model, which would be given by $\frac{(1-\alpha)\beta}{\gamma}$.

In the absence of the transport network, a simple upper bound for $R_0(\mathbf{x})$ would be given by the maximum R_0 value for a particular vertex. Based on the above results, we can see that introducing the commute network allows for further refinement of such an upper bound via the control of public transportation flows. Furthermore, the coupling between the home-work network and the transportation network means that minimizing such an upper bound is not as simple as reducing capacity on the route with the highest flow rate. Instead, it is necessary to account for flow *and* transmission rates together when determining the routes with the largest impact on the spread of the virus.

Beyond bounding the value of $R_0(\mathbf{x})$ for changing transport flows, we can also examine $\Delta R_0(\mathbf{x})$, which is serving as the constraint in the transport control problem. The following theorem provides bounds on the change in $R_0(\mathbf{x})$ that can be achieved simply by controlling \mathbf{x} :

Theorem 2. Assume we have a policy \mathbf{x} that is more restrained than having no intervention. Then at the disease free equilibrium $\Delta R_0(\mathbf{x}) = R_0(1) - R_0(\mathbf{x})$ satisfies

$$0 \leq \Delta R_0(\mathbf{x}) \leq \|\xi\|_{\ell^1} \|\eta\|_{\ell^1} \left(\frac{p_C(1-\alpha)}{\gamma} \right) \max_{v \in \mathcal{V}_{HW}} \sum_{w \in C^+(v)} p_{vw} \beta_w (1 - x_{vw}),$$

where ξ and η are the left and right eigenvectors of $G_0(1)$ normalized such that $\xi^\top \eta = 1$.

Proof. The inequality $0 \leq \Delta R_0(\mathbf{x})$ follows from Lemma 2. Taking norms on both sides of eq. (3) gives

$$|\Delta R_0(\mathbf{x})| \leq \|\xi\| \|\eta\| \|\Delta G_0(\mathbf{x})\|$$

for any induced matrix norm. Again choosing ℓ^1 , we have

$$\begin{aligned} \|\Delta G_0(\mathbf{x})\|_{\ell^1} &= \max_{v \in \mathcal{V}_{HW}} \sum_{u=1}^n [\Delta G_0(\mathbf{x})]_{uv} \\ &= \frac{p_C(1-\alpha)}{\gamma} \max_{v \in \mathcal{V}_{HW}} \sum_{w=1}^m p_{vw} \beta_w \left(\frac{\sum_{u=1}^n p_{uw} N_u}{[\rho_C(1)^\top N]_w} - \frac{x_{vw} \sum_{u=1}^n x_{uw} p_{uw} N_u}{[\rho_C(\mathbf{x})^\top N]_w} \right) \\ &= \frac{p_C(1-\alpha)}{\gamma} \max_{v \in \mathcal{V}_{HW}} \sum_{w=1}^m p_{vw} \beta_w (1 - x_{vw}), \end{aligned}$$

which gives the result. Note that each term in the sum is positive because of the definition of restrained policies. \square

In this result, the eigenvectors ξ and η encode the impact of network structure on the spread of disease, while the maximum over v accounts for worst-case transmission rates. Again, the coupling between disease transmission rates and public transportation flow rates means that simply restricting flow on the busiest lines is not guaranteed to have the largest impact on $R_0(\mathbf{x})$. However, it is possible to use these bounds to characterize potentially optimal policies:

Proposition 1. To maximize the upper bound (maximize the potential impact on R_0) we should choose a policy \mathbf{x} such that

$$\mathbf{x} = \arg \max_{\mathbf{x}} \left[\max_{v \in \mathcal{V}_{HW}} \sum_{w=1}^m p_{vw} \beta_w (1 - x_{vw}) \right].$$

The expression for \mathbf{x} here does not guarantee optimality, but it can be used to guide control strategies by characterizing the techniques that have the most potential impact. However, directly solving this argmax problem is infeasible for large networks, so it cannot replace the numerical methods implemented below. While the simpler expressions available at the disease-free equilibrium provide clearly interpretable bounds on $R_0(\mathbf{x})$ and $\Delta R_0(\mathbf{x})$, these results can be generalized to $R_t(\mathbf{x})$ and $\Delta R_t(\mathbf{x})$ as well.

Proposition 2. The basic reproduction number $R_t(\mathbf{x}) < 1$ for any $t \in [0, T]$ if and only if

$$\lim_{k \rightarrow \infty} G_t(\mathbf{x})^k = 0.$$

Proposition 2 holds due to the convergence of the power series of the NGM as R_0 is the spectral radius of NGM for any control \mathbf{x} . This condition has valuable practical meaning because $R_0 < 1$ is a central indicator that the infection cannot spread in a population.

In summary, solving for optimal flow control policies in eq.(4) or eq.(7) is computational challenging because of the nonlinear disease reproduction constraints. We can leverage general observations drawn above to improve computational efficiency. Besides, these observations also have important policy implications regarding transit-relate disease control plans.

4. Numerical results and case study

We validate the general rules for public transit control policies in Section 4.1 and test the impact of input data in Section 4.2. In Section 4.3, we present the improvement of control policy with monitoring feedback. To solve a case study of NYC’s subway system in Section 4.4, we investigate the impact of network complexity to shed light on solving the problem in large-scale commute networks.

4.1. Calibrating metapopulation and epidemic models

We combine multiple sources of data to design and calibrate a realistic metapopulation SEIR model with transit flows. Table 1 summarizes the epidemic model’s parameters from existing COVID-19 literature and the calibrated traffic flow data used in the rest of the numerical experiments. We consider an NYC case study because it has one of the world’s largest public transit systems that keeps providing essential transportation services during the COVID-19 pandemic. About 39% of the population in NYC use public transit for commuting, which is more than the population driving private cars (27%) (Tajalli and Hajbabaie, 2017). NYC was also one of the cities with the most COVID-19 cases in 2020. While the ridership of the subway witnessed a significant drop (Wang et al., 2020) amid the early stage of the epidemic, we hope to understand how a safe and effective management policy can help achieve a good trade-off between risk mitigation and mobility.

Parameter	Epidemic model			
	Average contagion rate β	Length of infectious period $1/\gamma$	Length of latent period δ	Quarantine ratio α
Value	0.422 (Prem et al., 2020)	6.5 days Yang et al. (2020)	5.1 days (Lauer et al., 2020)	0.15 (Nishiura et al., 2020)
Parameter	Public transit network			Constraint κ
	Origin-destination daily flow	Subway ridership in pandemic	Transit network transfer connectivity	
Source	Regional MTA (NYC, 2020)	Wang et al. (2020)	MTA (NYC, 2020)	
Parameter	Spatial SEIR weights (Clewlow and Laberteaux, 2016)			Constraint κ
	Hours active at home	Hours in work	Commute time	
Value	8 hr	8 hr	1 hr	0.5

Table 1: Parameters and data sources for NYC case study

We obtain the local infection rate β_v as follows:

$$\beta_v = \bar{\beta} \cdot \frac{d_v}{\bar{d}}, \quad \forall v \in \mathcal{V},$$

where $\bar{\beta}$ is the average contagion rate reported from the city-level aggregated analysis, d_v is the population density in region v and \bar{d} is the average population density.

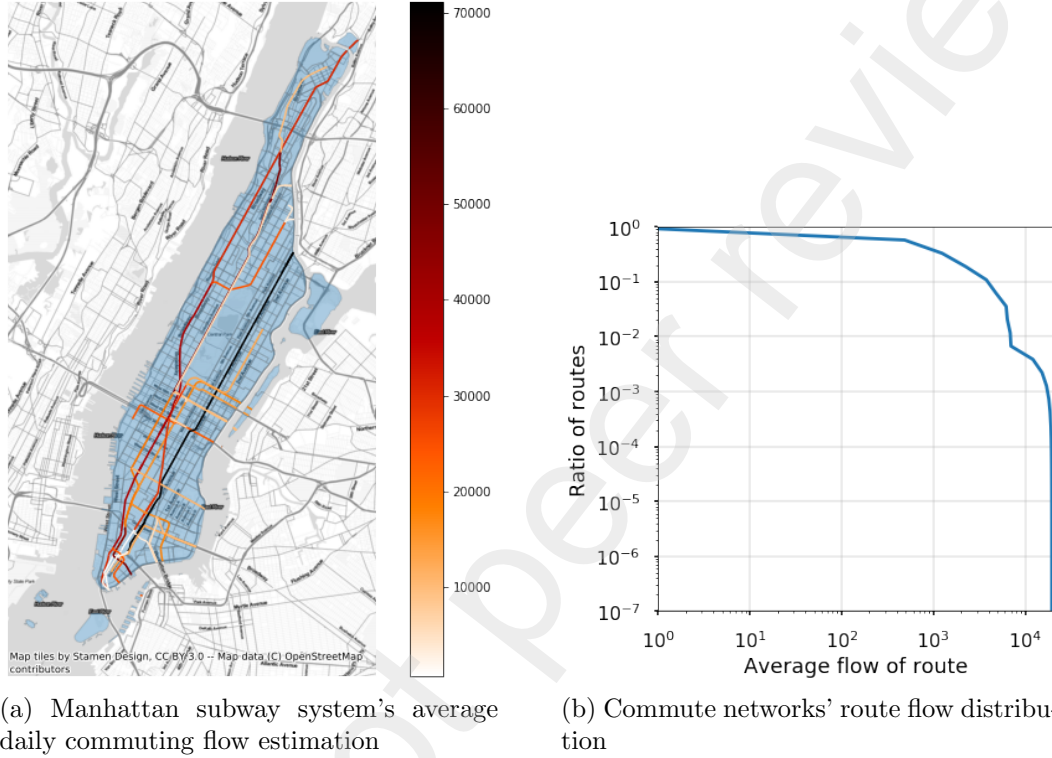


Figure 4: Case study: controlling public transit (subway) in Manhattan, NYC during the outbreak of COVID-19 in 2020.

Given the population N_v for $v \in \mathcal{V}_{HW}$ and daily commuting flows on the home-to-work network, we need to determine the probability of choosing each route p_{vw} for each $v \in \mathcal{V}_{HW}$ and $w \in \mathcal{V}_C$. We assume that each potential commuters behavior can be modeled via the following multinomial logit model (MNL):

$$p_{vw} = P(y = w | d_w) = \frac{\exp(\epsilon d_w)}{\sum_{w' \in \mathcal{V}_C} \exp(\epsilon d_{w'})},$$

where the Manhattan distance walking from the origin to nearest subway lines d_w is the single explanatory variable, y is the dependent variable for route choice, and ϵ is a constant depending on commuters' heterogeneity. Also, we assume that commuters use the same route from home to work and back (Yashima and Sasaki, 2016; Qian and Ukkusuri, 2020).

Each route's flow $w \in \mathcal{V}_C$ is $\sum_{v \in \mathcal{V}_{HW}} p_{vw} N_v$ and illustrated in Figure 4a. This route choice estimation is arguably inaccurate due to the lack of accurate movement data during the pandemic. We enhance the accuracy of route choice model by reweighing the routing

probabilities by the MTA subway ridership data NYC (2020). This is because trips other than commuting are also important components in the infectious contact in public transit. Section 4.2 shows that optimal control policies are insensitive to these estimation errors.

The recurring commuting patterns and the corresponding route-specific controls on public transit are necessary only if the density and the degree of the underlying commute network have a heavy-tailed distribution (Yashima and Sasaki, 2016). The distributional assumption is verified as the estimated distributions of the subway flow $\sum_{v \in \mathcal{V}_{HW}} p_{vw} N_v$ in Manhattan, NYC is obviously heavy-tailed in Figure 4b.

4.2. Aggregating commute networks and sensitivity analysis

We conduct three types of sensitivity analysis to understand the errors caused by model reductions and the input data inaccuracy. These tests are conducted on a small commute network of Figure C.14 in Appendix C).

- **Test on route choice:** A sensitivity analysis of the route choice model.
- **Test on commute network characteristics:** A sensitivity analysis of network properties such as the network degree.
- **Test on epidemic model:** A sensitivity analysis of the epidemic model's parameters.

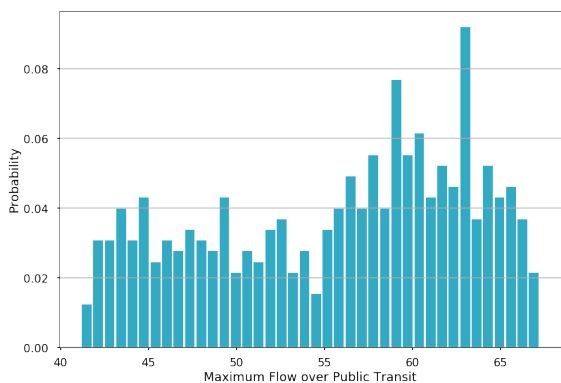
4.2.1. Sensitivity test on route choice

The first sensitivity analysis assumes that residents follow a random route choice model with a uniform distribution in this sample network. Unlike the distance-based choice model in the case study, we randomize the route choice to test how the lack of movement data access affects the transit control policy. We evaluate the variations of both objective and the reproduction rate of the emerging disease when people's route choice deviates from their daily routine before the epidemic.

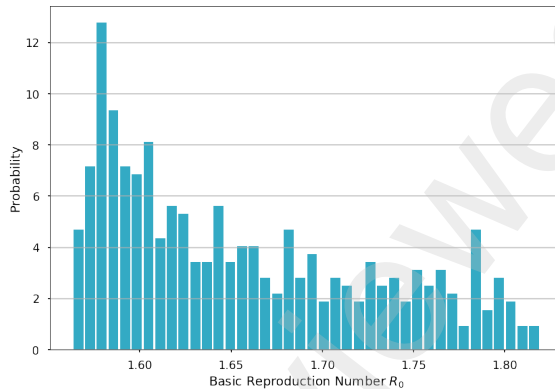
We simulate 1,000 experiments and repeatedly compute the optimal controls for public transit flow from eq.(4). The upper bound for the total transit throughput of about 85 depends on the sampled choice model. Note that, if there is no intervention in commute networks, i.e., $\mathbf{x} = 1$, the disease spreads with $R_0 = 1.75$; if the public transit is shut down, the disease is under control with $R_0 = 1.39$. Hence, the implementation of public transit flow controls is critical for public safety. We draw additional observations from this experiment:

1. The optimal control \mathbf{x} is small for regions with the large outflows and vice versa.
2. The objective and optimal controls \mathbf{x} is relatively sensitive to the uncertain route choice (Figure 5a) because p_{vw} are linear coefficients in the objective.
3. The disease reproduction constraint is also sensitive to the route choice model (Figure 5b).

We conclude that the accurate estimation for the route choice model is critical for the optimality of control plans. Hence, travel behavior changes during the on-peak and post-epidemic time are worth further investigation. The transportation authorities should be mindful of safe and reliable first- and last-mile connections to public transit during the epidemic outbreak.



(a) Effect on maximum flow



(b) Effect on basic reproduction number

Figure 5: Sensitivity of fixed optimal transit flow controls with regard to the random route choice

4.2.2. Test on commute network characteristics

We solve the fixed transit flow controls in eq.(4) by nonconvex programming with an increasing number of regions. Figure 6 shows that the computation time grows sub-exponentially as the size of the problem ($|\mathbf{x}| = |\mathcal{V}_{HW} \times \mathcal{V}_C|$) increases.

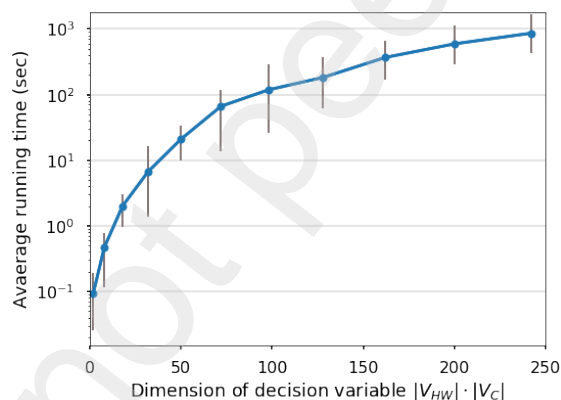


Figure 6: Optimization eq.(4)'s running time grows with the network size

Since the large-scale problem quickly becomes unsolvable, mainly due to the nonlinearity of the disease reproduction constraint, we are interested in reducing the complexity of the underlying commute network. This step is necessary for real-world problems such as the NYC case study. The commuter network in this study contains 288 census tract regions and 277 routes. Extrapolating the running time in Figure 6, computing the exact solution of the NYC network ($|\mathbf{x}| \approx 80,000$) by standard nonlinear programming methods is obviously impractical. For example, using the trust-region method (Byrd et al., 2000) to solve to optimally is expected to take $10^{15} - 10^{23}$ seconds on a standard computer (1.4GHz Intel i5, 8 GB RAM).

The complexity and the size of a commuter network are measured by the maximum network degree. As a fully connected commute network is assumed throughout the analysis, the degree of this network decreases when we aggregate regions into clusters. For example, when dividing the area evenly into two regions, the maximum degree of the network is 3,

and so on. To handle such a large-scale network analysis in the NYC case study, we can cluster regions in \mathcal{V}_{HW} with similar demographic information. Besides, we aggregate the inter-region commuting flows between these clusters. The question of optimality loss due to this vertex-aggregation procedure naturally arises. In the following experiment, we keep the constant total expected population $\|N\|_1 = 100$ when dividing the area of interest into finer and finer grids. As a result, the degree of commute network (i.e., the number of connections it has to other regions) increases from 2 to 16.

When the maximum degree of the commute network increases, the objective value of eq.(4) is stable, but the basic reproduction number increases significantly. The main reason is that the impact of critical regions is strengthened as the degree of network increases, and the basic reproduction number at optimality increases accordingly. This result supports the choice of relative measures on basic or effective reproduction number R_t over the absolute values in eq.(4) and eq.(7), respectively. In summary, the network throughput is unaffected by scaling the networks for computational efficiency, except that the control policies become less targeted.

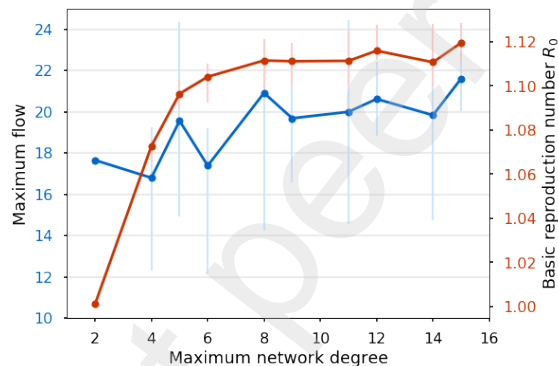


Figure 7: Sensitivity of the optimal control and the basic reproduction number regarding the commute network’s degree; Bars at each data point are the empirical variance from $M = 100$ experiments

4.2.3. Test on epidemic model parameters

The accuracy of the epidemic model is highly dependent on the estimated parameters in Table 1. However, these parameters, especially the contagion rate β_v from the susceptible population \mathbf{S}_t to the infected population \mathbf{I}_t , are affected by the anti-contagion policies (Hsiang et al., 2020) and social responsiveness (Chowdhury et al., 2020). For example, the transmission rate β reported in literature varies from 0.17 to 0.8 (Yang et al., 2020; Prem et al., 2020; Lauer et al., 2020; Wang et al., 2020) because of inaccurate data sources and the social distancing effect. We test the sensitivity of objective function in eq.(4) and basic reproduction number R_0 with varying parameters from the literature. The sensitivity test results are reported in Figure 8.

We draw the following observations from this sensitivity test:

1. As the average contagion rate $\bar{\beta}$ increases due to lack of prevention strategies such as social-distancing, the maximum public transit flow decreases to control the transmission. On the other hand, the basic reproduction number increases substantially.

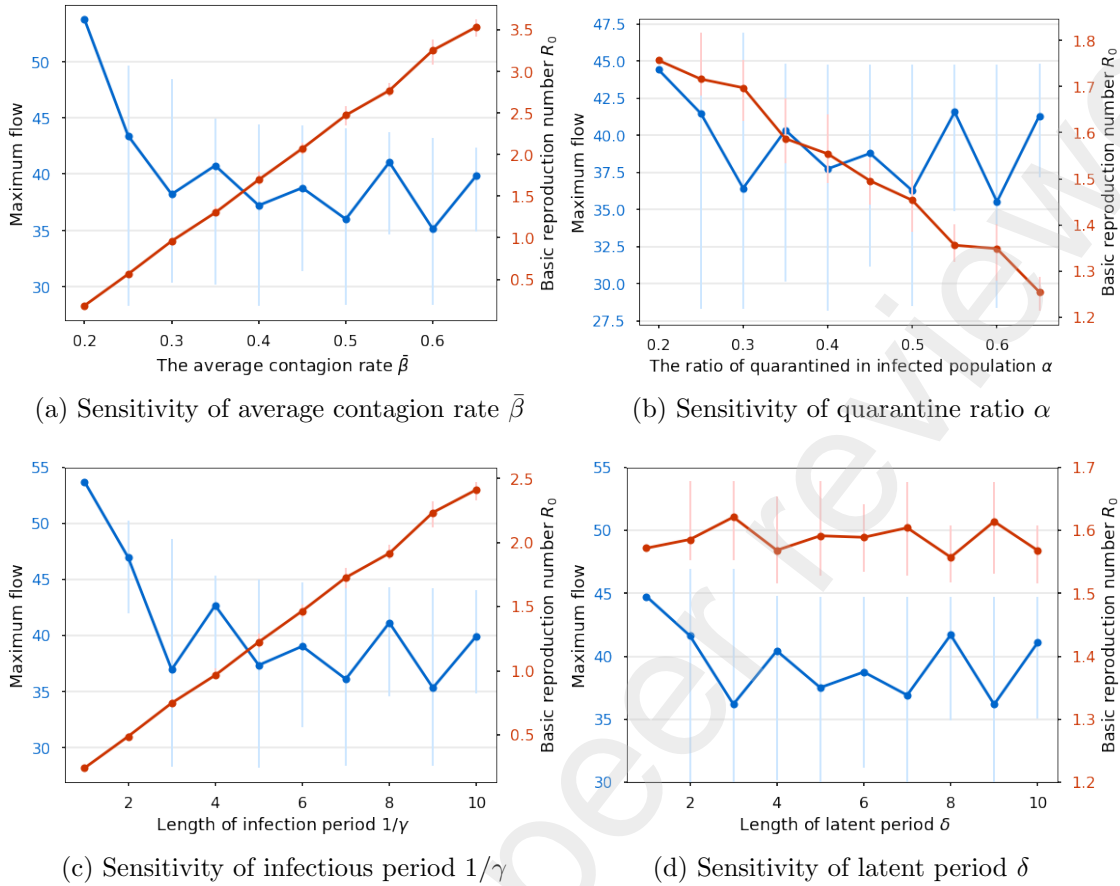


Figure 8: Sensitivity analysis of epidemic model parameters; Bars at each data point are the empirical variance from $M = 100$ experiments

2. As the quarantine ratio α increases, the maximum public transit flow stays approximately the same while the basic reproduction number decreases substantially. An example of this case is when the testing rate increases and the infected population is identified more effectively.
3. As the length of the infection period $1/\gamma$ increases due to healthcare quality deterioration, the maximum public transit flow decreases because of the significant increase in the basic reproduction number.
4. The latent period's length δ has a negligible impact on the optimal control policy or the disease spreading speed.

4.2.4. Social-distancing strategy on public transit

The contagion rate β_w is reduced for all $w \in \mathcal{V}_C$ when the public transit operator enforces stricter social-distancing policies for public transit. Such a policy can assist the control of the disease, as shown in Figure 9. To show the relative significance of implementing a social-distancing policy in public transit, we vary the ratio of $\beta_w/\bar{\beta}$. As a result, the basic disease reproduction number is reduced. Since eq.(4) and eq.(7) use relative disease reproduction constraints, the objective function is not much affected. To this end, social-distancing in public transit helps the public health measures and does not affect the maximal throughput

in commute networks.

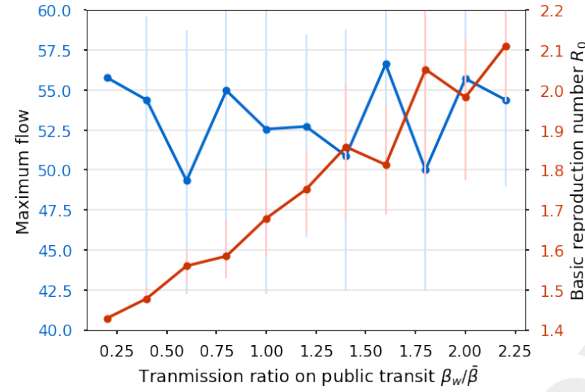


Figure 9: Effect of social-distancing policy on public transit; Bars at each data point are the empirical variance from $M = 100$ experiments

The value of κ in the disease reproduction constraint renders the safety-and-mobility trade-off. When κ increases from 0 to 1, the system puts more weight on efficiency and less weight on safety. As shown in Figure 10, the total throughput in commute networks increases significantly with larger κ . Note that the variation of the objective is considerable when κ is between 0.2 – 0.6. In the case study of NYC, the same trade-off is presented in the subway operational plans.

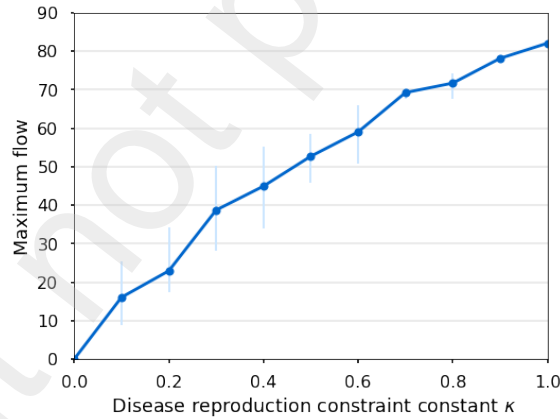


Figure 10: Safety-and-mobility trade-off; Bars at each data point are the empirical variance from $M = 100$ experiments

4.3. Numerical results for flow control with monitoring feedback

We demonstrate the insights obtained by solving a two-stage flow policy in the same network. The computation of the dynamic policy in Algorithm 1 allows to iteratively simulate the state \mathbf{S}_t and \mathbf{I}_t are dependent on $\mathbf{x}(\tau), \tau < t$. On the other hand, the disease reproduction constraints need to be satisfied for all $\tau \in \mathbf{T}$.

$\kappa(\tau)$ is a sequence of endogenous variables that mitigates the safety-and-mobility trade-off due to the evolving epidemic. As the constraint $\kappa_{R_0(0), R_0(1)}(t)$ is dependent on the realized

reproduction number at time t , the optimization automatically put more weights on economics than health concerns as the severeness of the disease relieves. Suppose that we make an initial flow control policy at $t = 0$ and allow to adjust the policy at $t' \in (0, T]$ when $R_{t'}(1)$ hits a preset threshold. To demonstrate the strictness of health measures associated with the basic reproduction number, we fix $\kappa(0) = 0.5$ and resolve the optimization eq (7) with different values of $\kappa_{R_{t'}(0), R_{t'}(1)}(t')$. Note that, as $\kappa_{R_{t'}(0), R_{t'}(1)}(t')$ increases, the second intervention is made earlier, and setting $\kappa(t') \approx 1.0$ is equivalent to relaxing the disease reproduction constraint.

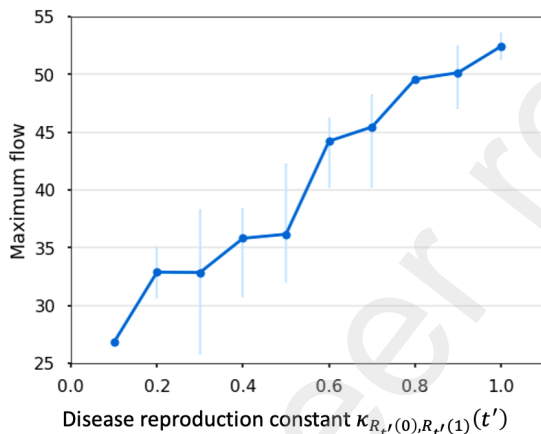


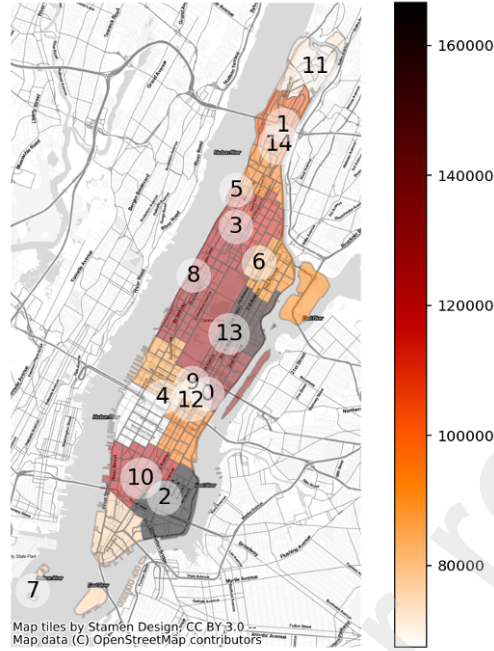
Figure 11: The optimal control when the health measures are relaxed over time; Bars at each data point are the empirical variance from $M = 20$ experiments

In Figure 11, the maximum flow over the public transit network increases as $\kappa_{R_{t'}(0), R_{t'}(1)}(t')$ increases, because the health measures are more critical for the disease control at the early stage. In other words, setting a large threshold for a sequential transit control decision increase the total throughput; thus, the transit agency’s quick responsiveness to the disease outbreak is valuable for social benefit. On each route and location, we also observe the inhomogeneous level of relieved flow in Figure C.15 in Appendix C when κ decreases or increases because eq.(7) automatically and effectively lifts the restrictions on transit traffic after the epidemic is under control.

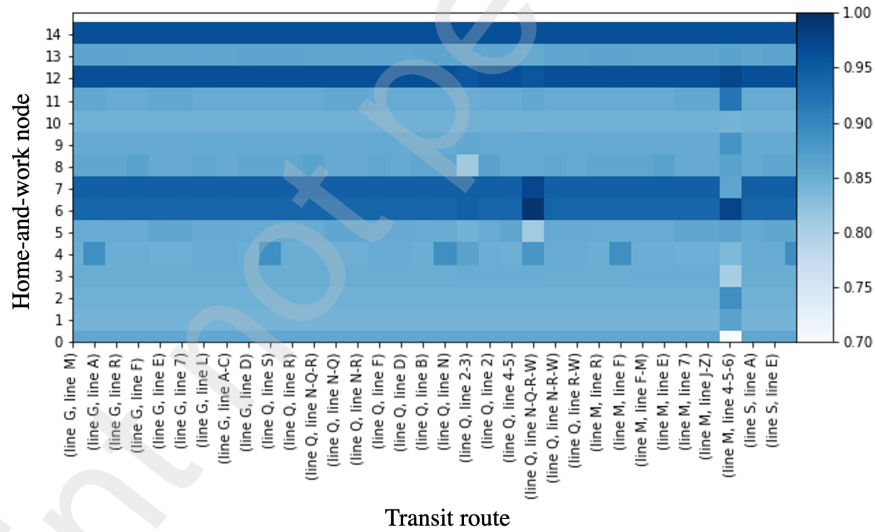
4.4. Safety-and-mobility trade-offs in NYC’s reopening decisions

Obtaining the control policy directly for complex urban infrastructure networks is computationally challenging. Due to the small optimality gap from the sensitivity test, optimizing a clustered commuter network does not influence the results’ generality. The census tracts in Manhattan, NYC are aggregated to 15 regions (labeled 0-14 in Figure 12a) by spatial clustering. Considering commuters’ transfers, the NYC subway system contains 277 combinations of subway lines, hence $|\mathcal{V}_C| = 277$ in the following analysis (transfers between subway lines can refer to Appendix C).

We focus on the fixed traffic flow control policy in this case study because the early interventions are more critical for safety in Section 4.3. The worst case that no intervention on public transit (i.e., $\mathbf{x} = 1$) is conducted, the basic reproduction number is $R_0(1) = 1.794$.



(a) Susceptible population N at $t = 0$ in aggregate home-and-work network \mathcal{V}_{HW}



(b) Optimal public transit control \mathbf{x}

Figure 12: Optimal public transit control policy in NYC case study

The most extreme case is a total closure of public transit (i.e., $\mathbf{x} = 0$), the basic reproduction number is $R_0(0) = 1.670$. The optimal control policy shown in Figure 12b obtains 88% (original network flow is 1.62 million) while reducing the gap of the basic reproduction rate at $R_0 = 1.703$.

Although the difference in basic reproduction number seems small, mainly due to the short time spent in transit per day p_C , the transit traffic control's effect on transmitting the infectious disease is significant. As we can see the epidemic dynamics in Figure 13,

the difference between the optimal control and no-control scenarios reaches 50,000 for the susceptible population and 30,000 for the infected population in Manhattan borough within the first $T = 100$ days of the outbreak. These results emphasize the need for controlling the disease transmission on the target region or public transit line during the reopening time, especially with the second-wave of COVID-19 pandemic worldwide (Leung et al., 2020).

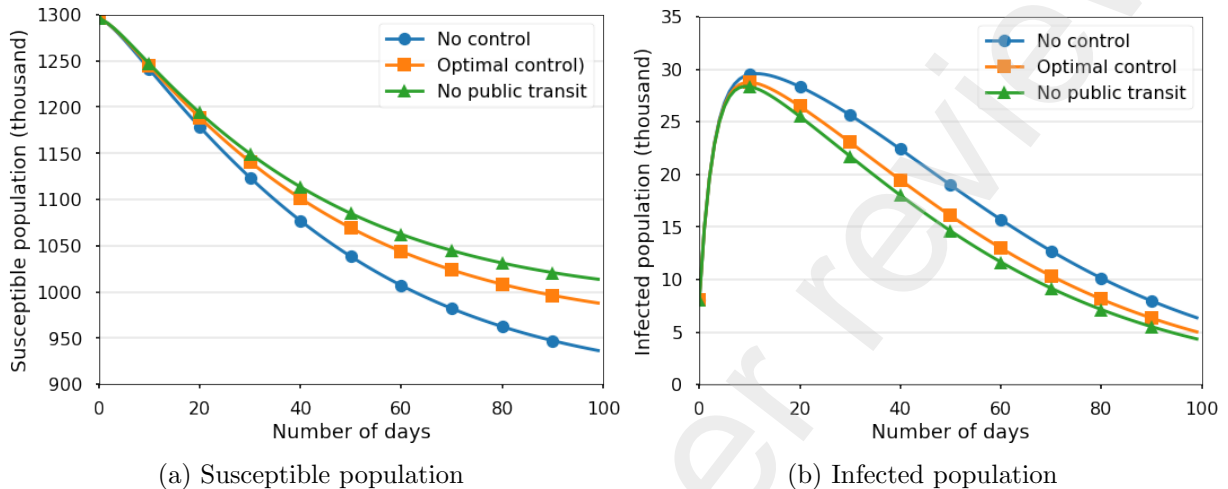


Figure 13: Dynamics of COVID-19 under different public transit control policies

Regarding the route-level controls in Figure 13b, we make two additional remarks on identifying the critical routes in transit traffic controls.

Remark 3 (Critical regions in commute networks). *In fully connected commute networks, the disease reproduction constraint is most sensitive to controls implemented on areas with largest outflow.*

Remark 4 (Route-based control). *Limiting flow on a high-density route does not necessarily control the spreading speed of the disease most effectively.*

Note that Remark 3 is consistent with the sensitivity analysis in Yashima and Sasaki (2016). The R_0 -centrality measure is defined as $-\frac{\partial \lambda_0(G)}{\partial N_v}$, which is equivalent to the sensitivity analysis on x_{vw} in the current work.

Finally, the numerical results of NYC case study provide several interesting policy implications that can be generalized to other cities' disease control plans:

1. The numerical results confirm the general rules derived in Section 3. For example, the optimal subway control policy is almost uniform on each row (corresponding to a home-and-work vertex) in Figure 12a. The most populated outflow vertex is curtailed the most.
2. Shutting down public transit, as passengers may choose alternative modes, brings marginal benefit comparing to the targeted traffic control policy in this work (Figure 13).

5. Conclusion

This paper proposes a mathematical programming approach under disease reproduction constraints to resolve safety-and-mobility trade-offs in epidemic response plans. An optimization-based analysis accommodates the essential demand for travel during the epidemic period and follows strict infectious disease safety measures. Public transit continues to serve as a protected, low-emission, and low-cost option for economic reopening by maximizing the transit flow restricted by the requirement of epidemic prevention measures.

This main limitation of this work is that, in extreme cases, the route-target public transit control policy has potential accessibility and equity problems. In the case study, transit flows on high-risk lines are reduced between 40% and 90% due to the relative demographic homogeneity in Manhattan, NYC. By either proposing new lower bounds for controls \mathbf{x} or reformulating the objective to a max-min problem, we can avoid this inequality issue. In order to capture the system's uncertainty, another promising research avenue is investigating more realistic models such as stochastic epidemic models and heterogeneous behavior models.

6. Acknowledgements

This material is based upon work supported by the National Science Foundation (NSF) under grant CMMI CIS 2033580 and U.S. Department of Transportation's University Transportation Centers Program. The authors would like to thank Juan Carlos Martinez Mori and Doreen Gui at Cornell University and William Barbour at Vanderbilt University for their assistance and advise. The contents of this report reflect the views of the authors, who are responsible for the facts and the accuracy of the information presented herein. This document is disseminated in the interest of information exchange. The report is funded, partially or entirely, by a grant from the U.S. Department of Transportation's University Transportation Centers Program. However, the U.S. Government assumes no liability for the contents or use thereof.

References

- Amekudzi-Kennedy, A., Labi, S., Woodall, B., Chester, M., Singh, P., 2020. Reflections on pandemics, civil infrastructure and sustainable development: Five lessons from covid-19 through the lens of transportation .
- Balcan, D., Vespignani, A., 2011. Phase transitions in contagion processes mediated by recurrent mobility patterns. *Nature physics* 7, 581–586.
- Bhatia, R., 2007. Perturbation bounds for matrix eigenvalues. SIAM.
- Bichara, D., Iggidr, A., 2018. Multi-patch and multi-group epidemic models: a new framework. *Journal of mathematical biology* 77, 107–134.
- Byrd, R.H., Gilbert, J.C., Nocedal, J., 2000. A trust region method based on interior point techniques for nonlinear programming. *Mathematical programming* 89, 149–185.

- Chang, S.Y., Pierson, E., Koh, P.W., Gerardin, J., Redbird, B., Grusky, D., Leskovec, J., 2020. Mobility network modeling explains higher sars-cov-2 infection rates among disadvantaged groups and informs reopening strategies. medRxiv URL: <https://www.medrxiv.org/content/early/2020/06/17/2020.06.15.20131979>, doi:10.1101/2020.06.15.20131979, arXiv:<https://www.medrxiv.org/content/early/2020/06/17/2020.06.15.20131979>
- Chin, A.W., Chu, J.T., Perera, M.R., Hui, K.P., Yen, H.L., Chan, M.C., Peiris, M., Poon, L.L., 2020. Stability of sars-cov-2 in different environmental conditions. *The Lancet Microbe* 1, e10.
- Chowdhury, R., Heng, K., Shawon, M.S.R., Goh, G., Okonofua, D., Ochoa-Rosales, C., Gonzalez-Jaramillo, V., Bhuiya, A., Reidpath, D., Prathapan, S., et al., 2020. Dynamic interventions to control covid-19 pandemic: a multivariate prediction modelling study comparing 16 worldwide countries. *European journal of epidemiology* 35, 389–399.
- Clewlow, R., Laberteaux, K., 2016. Shared-use mobility in the united states: Current adoption and potential impacts on travel behavior, in: 95th Annual Meeting of the Transportation Research Board (TRB), Washington DC, United States.
- Cohen, J., Kupferschmidt, K., 2020. Countries test tactics in 'war' against covid-19. *Science* 367, 1287.
- DeWeese, J., Hawa, L., Demyk, H., Davey, Z., Belikow, A., El-geneidy, A., 2020. A tale of 40 cities: A preliminary analysis of equity impacts of covid-19 service adjustments across north america. *Transport Findings* doi:10.32866/001c.13395.
- van Dorn, A., Cooney, R.E., Sabin, M.L., 2020. Covid-19 exacerbating inequalities in the us. *The Lancet* 395, 1243–1244.
- Feng, S., Shen, C., Xia, N., Song, W., Fan, M., Cowling, B.J., 2020. Rational use of face masks in the covid-19 pandemic. *The Lancet Respiratory Medicine* 8, 434–436.
- Hsiang, S., Allen, D., Annan-Phan, S., Bell, K., Bolliger, I., Chong, T., Druckenmiller, H., Huang, L.Y., Hultgren, A., Krasovich, E., et al., 2020. The effect of large-scale anti-contagion policies on the covid-19 pandemic. *Nature* , 1–9.
- Hu, Y., Barbour, W., Samaranyake, S., Work, D., 2020. Impacts of covid-19 mode shift on road traffic. arXiv preprint arXiv:2005.01610 .
- Keeling, M.J., Danon, L., Vernon, M.C., House, T.A., 2010. Individual identity and movement networks for disease metapopulations. *Proceedings of the National Academy of Sciences* 107, 8866–8870.
- Lauer, S.A., Grantz, K.H., Bi, Q., Jones, F.K., Zheng, Q., Meredith, H.R., Azman, A.S., Reich, N.G., Lessler, J., 2020. The incubation period of coronavirus disease 2019 (covid-19) from publicly reported confirmed cases: estimation and application. *Annals of internal medicine* 172, 577–582.

- Lee, S.G., Hickman, M., 2014. Trip purpose inference using automated fare collection data. *Public Transport* 6, 1–20.
- Leung, K., Wu, J.T., Liu, D., Leung, G.M., 2020. First-wave covid-19 transmissibility and severity in china outside hubei after control measures, and second-wave scenario planning: a modelling impact assessment. *The Lancet* .
- Lewnard, J.A., Lo, N.C., 2020. Scientific and ethical basis for social-distancing interventions against covid-19. *The Lancet. Infectious diseases* .
- McLaren, J., 2020. Racial Disparity in COVID-19 Deaths: Seeking Economic Roots with Census data. Technical Report. National Bureau of Economic Research.
- Mo, B., Feng, K., Shen, Y., Tam, C., Li, D., Yin, Y., Zhao, J., 2020. Modeling epidemic spreading through public transit using time-varying encounter network. arXiv preprint arXiv:2004.04602 .
- Mori, J.C.M., Barbour, W., Gui, D., Piccoli, B., Work, D., Samaranyake, S., 2020. A multi-region seir model with mobility. <https://seir.cee.cornell.edu>.
- Nishiura, H., Kobayashi, T., Miyama, T., Suzuki, A., Jung, S.m., Hayashi, K., Kinoshita, R., Yang, Y., Yuan, B., Akhmetzhanov, A.R., et al., 2020. Estimation of the asymptomatic ratio of novel coronavirus infections (covid-19). *International journal of infectious diseases* 94, 154.
- NYC, M., 2020. The metropolitan transportation authority of new york city. <http://web.mta.info/mta/planning/data.html>. Last accessed on July 10, 2020.
- Prem, K., Liu, Y., Russell, T.W., Kucharski, A.J., Eggo, R.M., Davies, N., Flasche, S., Clifford, S., Pearson, C.A., Munday, J.D., et al., 2020. The effect of control strategies to reduce social mixing on outcomes of the covid-19 epidemic in wuhan, china: a modelling study. *The Lancet Public Health* .
- Qian, X., Sun, L., Ukkusuri, S.V., 2020. Scaling of contact networks for epidemic spreading in urban transit systems. arXiv preprint arXiv:2002.03564 .
- Qian, X., Ukkusuri, S.V., 2020. Modeling the spread of infectious disease in urban areas with travel contagion. arXiv preprint arXiv:2005.04583 .
- Tajalli, M., Hajbabaie, A., 2017. On the relationships between commuting mode choice and public health. *Journal of Transport & Health* 4, 267–277.
- Van Doremalen, N., Bushmaker, T., Morris, D.H., Holbrook, M.G., Gamble, A., Williamson, B.N., Tamin, A., Harcourt, J.L., Thornburg, N.J., Gerber, S.I., et al., 2020. Aerosol and surface stability of sars-cov-2 as compared with sars-cov-1. *New England Journal of Medicine* 382, 1564–1567.
- Wang, D., He, B.Y., Gao, J., Chow, J.Y., Ozbay, K., Iyer, S., 2020. Impact of covid-19 behavioral inertia on reopening strategies for new york city transit. arXiv preprint arXiv:2006.13368 .

Yang, Z., Zeng, Z., Wang, K., Wong, S.S., Liang, W., Zanin, M., Liu, P., Cao, X., Gao, Z., Mai, Z., et al., 2020. Modified seir and ai prediction of the epidemics trend of covid-19 in china under public health interventions. *Journal of Thoracic Disease* 12, 165.

Yashima, K., Sasaki, A., 2016. Spotting epidemic keystones by r_0 sensitivity analysis: High-risk stations in the tokyo metropolitan area. *PLoS one* 11, e0162406.

Zhou, Y., Wang, J., Yang, H., 2019. Resilience of transportation systems: concepts and comprehensive review. *IEEE Transactions on Intelligent Transportation Systems* .

Appendix A. Summary of notation

Table A.2: Summary of notation

Notation	Definition
Spatial SEIR model	
\mathcal{G}_{HW}	Home-and-work network consists of vertices (regions) \mathcal{V}_{HW} and edges \mathcal{E}_{HW}
\mathcal{G}_C	Public transit network consists of vertices \mathcal{V}_C and edges \mathcal{E}_C
\mathcal{G}	Commute network integrates \mathcal{G}_{HW} and \mathcal{G}_C
N_v	Population in region $v \in \mathcal{V}_{HW}$
$\mathcal{N}^+(v)$	A set of neighboring outflow regions and $\mathcal{N}^+(v) \subset \mathcal{V}_{HW}$
$\mathcal{N}^-(v)$	A set of neighboring inflow regions and $\mathcal{N}^-(v) \subset \mathcal{V}_{HW}$
$\mathcal{C}^+(v)$	A set of neighboring outflow and $\mathcal{C}^+(v) \subset \mathcal{V}_C$
$\mathcal{C}^-(v)$	A set of neighboring inflow and $\mathcal{C}^-(v) \subset \mathcal{V}_C$
$N_v^e(t)$	Effective work-home population
$C_v^e(t)$	Effective commuting population
ρ_N	Daily home-to-work flow fraction matrix with entries r_{uv}
ρ_C	Transit flow fraction matrix with entries p_{uv}
\mathbf{S}_t	Vector of susceptible population
\mathbf{E}_t	Vector of exposed population
\mathbf{I}_t	Vector of infectious population
\mathbf{R}_t	Vector of recovered population
β_v	Contact rate at vertex $v \in \mathcal{V}$
γ	Recovering rate of the disease
$1/\delta$	Mean latent period of the disease
α	Quarantine ratio
p_H, p_W, p_C	Proportion of time during the day spent at home, work, and commute vertices, respectively
R_0	Basic reproduction number
G_0	Next generation matrix
R_t	Effective reproduction number
Optimization model	
\mathbf{x}	Decision variable for static transit flow control x_{vw} for all $v \in \mathcal{V}_{HW}$ and $w \in \mathcal{V}_C$
κ	Tolerance for the disease reproduction constraint in the static control policy
ζ, η	Left and right eigenvectors associated with R_t
τ	The time period flow controls are implemented
$\Delta\tau$	Time duration each control is implemented
$\kappa_{R_\tau(0), R_\tau(1)}(\tau)$	Tolerance for the disease reproduction constraint in the control policy

Appendix B. Proof for the compartment model

Computing the next generation matrix (NGM) is a central task for computing R_0 . To compute the next generation matrix, we actually only care about the *infected subsystem*, the set of populations that contain infected individual consisting of $E_v(t)$ and $I_v(t)$ for all regions $v \in \mathcal{V}$. To compute the Jacobian, we need to compute $\frac{\partial}{\partial E_v} \left(\frac{dE_u}{dt} \right)$, $\frac{\partial}{\partial I_v} \left(\frac{dE_u}{dt} \right)$, $\frac{\partial}{\partial E_v} \left(\frac{dI_u}{dt} \right)$, $\frac{\partial}{\partial I_v} \left(\frac{dI_u}{dt} \right)$, where each is evaluated at $S_u = N_u$ and $I_u = 1$. We collect the terms as follows:

$$\begin{aligned}
 [J]_{E_v E_v} &= \frac{\partial}{\partial E_v} \left(\frac{dE_v}{dt} \right) = -\frac{1}{\delta} \\
 [J]_{E_u E_v} &= \frac{\partial}{\partial E_v} \left(\frac{dE_u}{dt} \right) = 0 \\
 [J]_{I_v E_v} &= \frac{\partial}{\partial E_v} \left(\frac{dI_v}{dt} \right) = \frac{1}{\delta} \\
 [J]_{I_u E_v} &= \frac{\partial}{\partial E_v} \left(\frac{dI_u}{dt} \right) = 0 \\
 [J]_{I_v I_v} &= \frac{\partial}{\partial I_v} \left(\frac{dI_v}{dt} \right) = -\gamma \\
 [J]_{I_u I_v} &= \frac{\partial}{\partial I_v} \left(\frac{dI_u}{dt} \right) = 0 \\
 [J]_{E_v I_v} &= \frac{\partial}{\partial I_v} \left(\frac{dE_v}{dt} \right) = -\frac{\partial}{\partial I_v} \left(\frac{dS_v}{dt} \right) \\
 &= p_H \beta_v (1 - \alpha) \frac{S_v}{N_v} + p_W \sum_{u \in \mathcal{N}^+(v)} r_{vu}^2 \beta_u \frac{(1 - \alpha) S_v [\rho_N^\top N]_u}{([\rho_N^\top N]_u)^2} \\
 &\quad + p_C \sum_{w \in \mathcal{C}^+(v)} x_{vw}^2 p_{vw}^2 \beta_w \frac{(1 - \alpha) S_v [\rho_C(x)^\top C]_w}{([\rho_C(x)^\top C]_w)^2} \\
 [J]_{E_u I_v} &= \frac{\partial}{\partial I_v} \left(\frac{dE_u}{dt} \right) = -\frac{\partial}{\partial I_v} \left(\frac{dS_u}{dt} \right) \\
 &= p_W \sum_{w \in \mathcal{N}^+(u) \cap \mathcal{N}^+(v)} \beta_w r_{uw} r_{vw} \frac{(1 - \alpha) S_v [\rho_N^\top N]_w}{([\rho_N^\top N]_w)^2} \\
 &\quad + p_C \sum_{w \in \mathcal{C}^+(u) \cap \mathcal{C}^+(v)} \beta_w x_{uw} p_{uw} x_{vw} p_{vw} \frac{(1 - \alpha) S_v [\rho_C(x)^\top C]_w}{([\rho_C(x)^\top C]_w)^2}
 \end{aligned}$$

Note there exists a disease-free equilibrium with $S_v = N_v$ and $I_v = 0$ for all $v \in \mathcal{V}$. In the case of fixed control, we can directly plug in these values to further simplify the computation. Note both F and V in dimension $\mathbb{R}^{2|\mathcal{V}| \times 2|\mathcal{V}|}$ and hence we can write the NGM as:

$$G = FV^{-1}|_{>0} \quad (\text{B.1})$$

$$[F]_{uv} = \begin{cases} p_H \beta_v (1 - \alpha) + p_W \sum_{u \in \mathcal{N}^+(v)} r_{vu}^2 \beta_u \frac{(1-\alpha)N_v [\rho_N^T N]_u}{([\rho_N^T N]_u)^2} + \\ p_C \sum_{w \in \mathcal{C}^+(v)} x_{vw}^2 p_{vw}^2 \beta_w \frac{(1-\alpha)N_v [\rho_C(x)^T C]_w}{([\rho_C(x)^T C]_w)^2}, & u = v, u, v \in \mathcal{V} \\ p_W \sum_{w \in \mathcal{N}^+(u) \cap \mathcal{N}^+(v)} \beta_w r_{uw} r_{vw} \frac{(1-\alpha)N_v [\rho_N^T N]_w}{([\rho_N^T N]_w)^2} + \\ p_C \sum_{w \in \mathcal{C}^+(u) \cap \mathcal{C}^+(v)} \beta_w x_{uw} p_{uw} x_{vw} p_{vw} \frac{(1-\alpha)N_v [\rho_C(x)^T C]_w}{([\rho_C(x)^T C]_w)^2}, & u \neq v, u, v \in \mathcal{V} \end{cases}, \quad (\text{B.2})$$

$$V = \begin{bmatrix} \frac{1}{\delta} & \cdots & 0 & 0 & \cdots & 0 \\ \vdots & \ddots & \vdots & \vdots & \ddots & \vdots \\ 0 & \cdots & \frac{1}{\delta} & 0 & \cdots & 0 \\ \frac{1}{\delta} & \cdots & 0 & \gamma & \cdots & 0 \\ \vdots & \ddots & \vdots & \vdots & \ddots & \vdots \\ 0 & \cdots & \frac{1}{\delta} & 0 & \cdots & \gamma \end{bmatrix}. \quad (\text{B.3})$$

If we compute the expanded G from these expression for F and V^{-1} we get

$$G = FV^{-1}|_{>0} = \begin{bmatrix} 0 & \cdots & 0 & \frac{1}{\gamma} [F]_{E_v I_v} & \cdots & \frac{1}{\gamma} [F]_{E_u I_v} \\ \vdots & \ddots & \vdots & \vdots & \ddots & \vdots \\ 0 & \cdots & 0 & \frac{1}{\gamma} [F]_{E_u I_v} & \cdots & \frac{1}{\gamma} [F]_{E_v I_v} \\ 0 & \cdots & 0 & 0 & \cdots & 0 \\ \vdots & \ddots & \vdots & \vdots & \ddots & \vdots \\ 0 & \cdots & 0 & 0 & \cdots & 0 \end{bmatrix} |_{>0} \quad (\text{B.4})$$

and here the nonzero submatrix is the NGM, G . We can see that:

$$[G]_{vv} = \frac{1}{\gamma} [F]_{E_v I_v} \quad (\text{B.5})$$

$$[G]_{vu} = \frac{1}{\gamma} [F]_{E_u I_v} \quad (\text{B.6})$$

Appendix C. Commute networks in NYC numerical experiments

In the sensitivity analysis, the simulations use the following commute network ($|\mathcal{V}_{HW}| = 4, |\mathcal{V}_C| = 6$) with randomly generated population (with expected total population of 100) and route choice. The flow between each pair of regions $u, v \in \mathcal{V}$ are sorted from high to low by the home-and-work vertex index. The values are represented by the line opacity in Figure C.14.

The route-based control policy for the flow control numerical experiments is shown in Figure C.15. The underlying commute graph is the same as in Figure C.14. The epidemic model's parameters follow the NYC cast study in Table 1. We evaluate the control policy in this relatively small network, mainly because of the epidemic dynamic model's computational

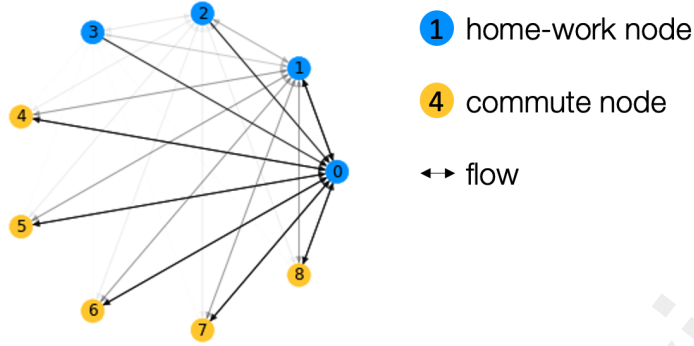
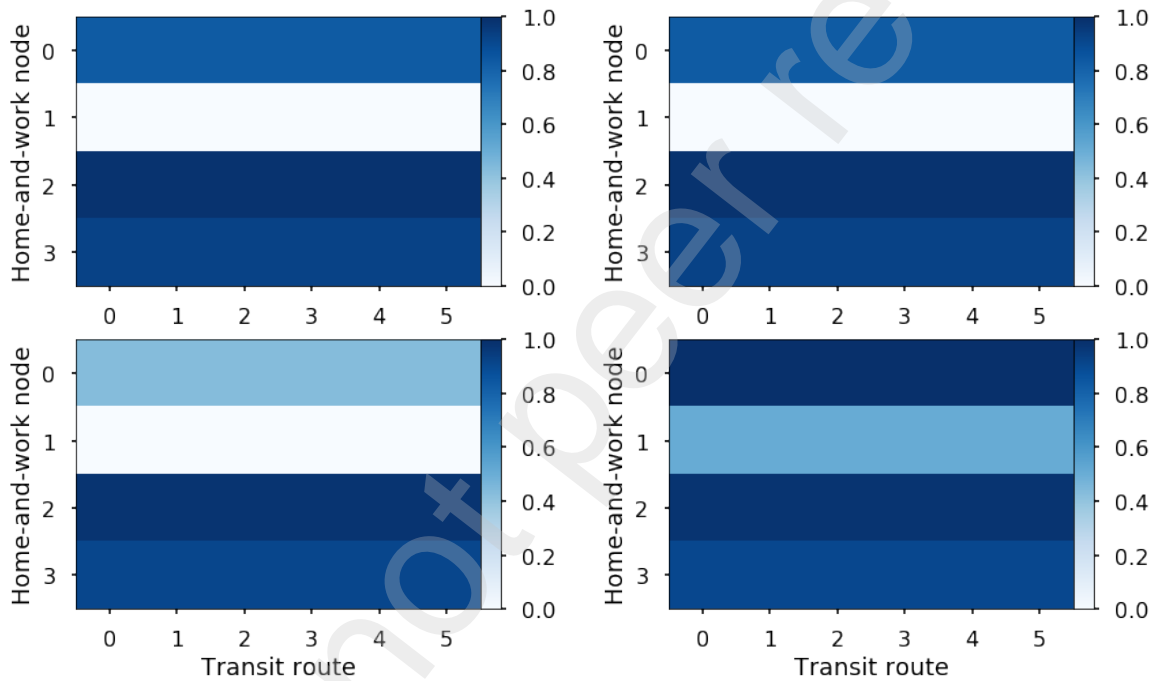


Figure C.14: Commute network for control policy validation



(a) At $t = 0$ (up) with $\kappa(0) = 0.5$ and $t' > 0$ (down) with $\kappa(t') = 0.2$. (b) At $t = 0$ (up) with $\kappa(0) = 0.5$ and $t' > 0$ (down) with $\kappa(t') = 0.9$.

Figure C.15: Optimal transit flow control $\mathbf{x}^*(t)$ with different strictness of health measures

limitation. Since we are interested in the potential of the policy with monitoring feedback compared to the fixed policy in this experiment, the derived results are general.

The connectivity of the subway system is required for constructing the commute network in the NYC case study. Considering only the individual physical transit lines are not an appropriate vertex representation in the commuter network. Infected passengers may transfer between lines in a single trip and cause contagion on all visited lines. By limiting the number of transfers to one, we can crawl the public transit data NYC (2020) to reconstruct the commute network transfer graph as in Figure C.16. Each edge connecting two subway lines are treated as a vertex $w \in \mathcal{V}_C$.

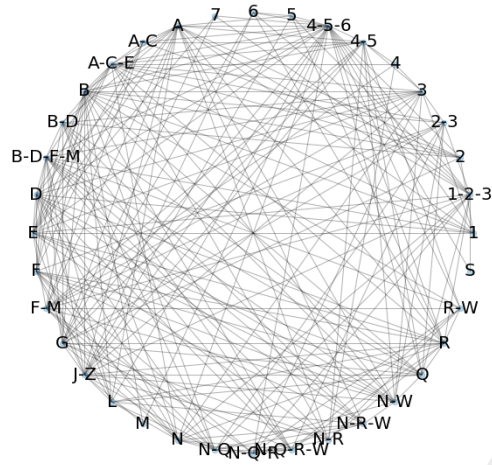


Figure C.16: Connectivity of the MTA subway systems in NYC; Each edge in the graph is $v \in \mathcal{V}_C$ in the commute network